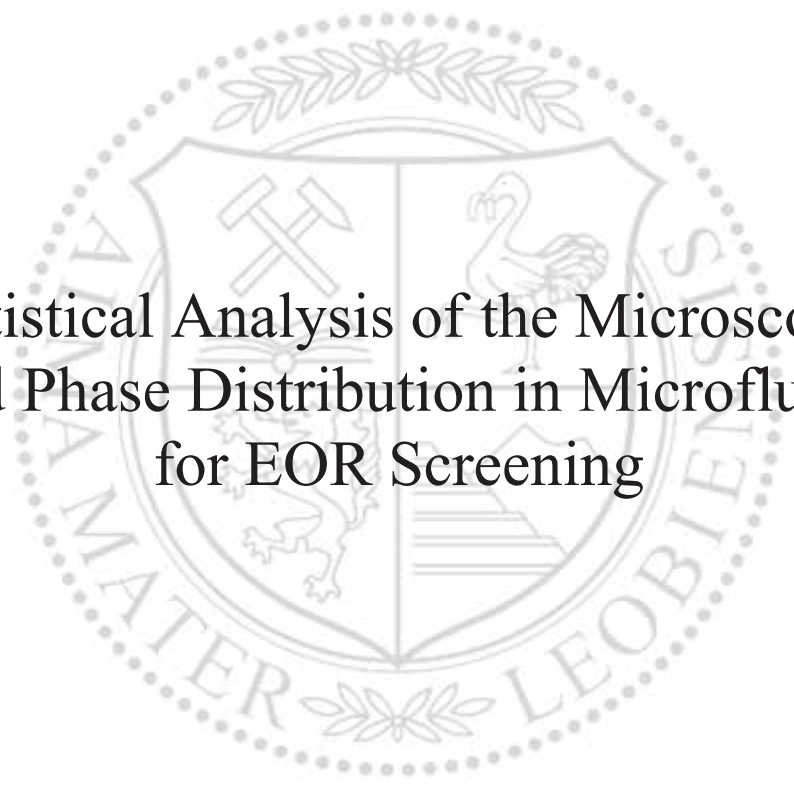




Chair of Reservoir Engineering

Master's Thesis

The background features a large, faint watermark of the University of Leoben seal. The seal is circular and contains a shield with various symbols: a hammer and pickaxe, a stork, a lion, and a pyramid. The text 'UNIVERSITAS MONTANA LEOBENSIS' is visible around the perimeter of the seal.

Statistical Analysis of the Microscopic
Fluid Phase Distribution in Microfluidics
for EOR Screening

Barbara Schnöpf, BSc

May 2019

Barbara Schnöpf

Master Thesis 2019

Supervisor: Univ.-Prof. Dipl.-Phys. Dr.rer.nat. Holger Ott

Statistical Analysis of the Microscopic Fluid Phase Distribution in Microfluidics for EOR Screening

To my beloved friends who became my family

Declaration

I hereby declare that except where specific reference is made to the work of others, the contents of this dissertation are original and have not been published elsewhere. This dissertation is the outcome of my own work using only cited literature.

Erklärung

Hiermit erkläre ich, dass der Inhalt dieser Dissertation, sofern nicht ausdrücklich auf die Arbeit Dritter Bezug genommen wird, ursprünglich ist und nicht an anderer Stelle veröffentlicht wurde. Diese Dissertation ist das Ergebnis meiner eigenen Arbeit mit nur zitierter Literatur.



Barbara Schnöpf, 24 May 2019

Acknowledgements

I want to sincerely thank my supervisor Prof. Holger Ott for teaching and guiding me through my thesis with his tremendous knowledge and providing me with the opportunity of this research work.

In addition, I want to thank the whole Reservoir Engineering Team for their support, especially Ahmad Kharrat and Pit Arnold who challenged and motivated me regularly throughout the past couple of months as well as Kata Kurgyis and Mostafa Borji for their moral support.

Abstract

Alkaline flooding, as one of the chemical EOR processes, modifies the properties of fluid-fluid as well as rock-fluid interfaces in the reservoir in order to mobilize additional oil.

In this thesis, observations on the pore scale were recorded and analysed to provide information on the displacement mechanism of brine and alkaline flooding which was applied to crude oil. The alkaline concentration ranged from 200ppm to 12000ppm.

Microfluidics were used to visualize the dynamic oil distribution in the pore space and the formation of emulsion phases. In means of the statistical analysis, the Lorenz plot and normalized Euler characteristic were applied.

Phase behaviour experiments provided additional information about the different phases and formation of emulsions. The experiments were carried out at ambient temperature conditions as well as reservoir temperature conditions to attain a more realistic approach. For some cases, a spinning drop measurement additionally provided data on interfacial tension.

The highest ultimate recovery was achieved at ambient temperature conditions in the flooding scenario of synthetic brine with 12000ppm alkaline salt, which resulted in an oil-wet system. An entirely water-wet system was only achieved by using deionized water in combination with alkaline salt.

Temperature flooding experiments were carried out with brine and deionized water, each in solution with 3000ppm alkaline salt, since this was initially assumed to be an ideal concentration due to promising results with another oil in the same field.

The phase behaviour experiment of synthetic water with 5000ppm alkaline salt showed an optimum at reservoir temperature conditions. There was no comparable behaviour found at ambient temperature conditions which emphasizes the great effect that temperature has on mixing conditions.

Zusammenfassung

Alkaliflutungen werden häufig angewendet um zusätzliches Öl zu produzieren. Sie sind eine Art von chemischer Enhanced Oil Recovery (EOR) die durch Veränderung einiger Eigenschaften zwischen verschiedenen Flüssigkeiten aber auch Flüssigkeiten und Gesteinsoberflächen ermöglichen zusätzliches Öl zu mobilisieren.

In dieser Arbeit wurden mithilfe von Mikrofluidik Beobachtungen aufgezeichnet um Informationen über Verdrängungsprozesse der Wasser- und Alkaliflutung zu vergleichen. Rohöl wurde durch synthetisches Wasser mit Alkalikonzentrationen von 200ppm bis 12000ppm verdrängt. Mikrofluidik ermöglichte es die dynamische Verteilung von Öl und Wasser im porösen Medium zu beobachten, sowie die Bildung von Emulsionen zwischen Öl und Wasser. Zur statistischen Auswertung wurden Ergebnisse grafisch in einem Lorenz Plot und mithilfe einer normalisierten Euler Charakteristik zusammengefasst.

Experimente zum Phasenverhalten lieferten weitere Informationen zu der Bildung von Emulsionen unter verschiedenen Bedingungen. Die Experimente wurden bei Umgebungstemperatur und Lagerstättentemperatur ausgeführt um eine realistische Vorgehensweise zu erzeugen. In manchen Fällen wurde auch die Grenzflächenspannung mittels einer Spinning Drop Methode gemessen.

Die höchste Ölgewinnung wurde bei Umgebungstemperatur und 12000ppm Alkali Salz gelöst in synthetischem Wasser erzielt. Dieses Experiment war nach der Alkaliflutung Öl benetzt. Der einzige Fall in welchem ein zu Gänze Wasser benetztes System entstand, war der Versuch in welchem nur entionisiertes Wasser in Lösung mit Alkali Salz angewendet wurde.

Die Flutungsexperimente bei Lagerstättentemperatur wurden mit Salzwasser und entionisiertem Wasser jeweils in Lösung mit 3000ppm Alkali Salz durchgeführt, da diese Konzentration ursprünglich als ideal angesehen wurde nachdem sie bei einem anderen Öl im selben Feld sehr erfolgreich war.

Später wurde in Folge ein optimaler Zustand in einem Phasenverhaltensexperiment bei Lagerstättentemperatur mit 5000ppm Alkali Salz in synthetischem Wasser gelöst, gefunden. Es konnte kein optimaler Zustand in den verwandten Versuchen bei Umgebungstemperatur gefunden werden. Dies betont großen Einfluss der Temperatur auf das Mischverhalten zwischen Öl und Wasser.

Table of Contents

Declaration.....	iii
Acknowledgements.....	iv
Abstract.....	v
Zusammenfassung.....	vi
<u>Chapter 1</u> Introduction.....	11
1.1 Background and Context.....	11
1.2 Scope and Objectives.....	12
<u>Chapter 2</u> Literature Review.....	13
2.1 Enhanced Oil Recovery.....	13
2.2 Chemical Flooding.....	13
2.3 Phase Behaviour.....	16
<u>Chapter 3</u> Experimental Devices and Equipment.....	19
3.1 Micromodel and Microscope.....	19
3.2 Temperature Setup.....	20
3.3 Injection Equipment.....	21
3.4 Additional Equipment.....	21
<u>Chapter 4</u> Methodology.....	23
4.1 Microfluidic Experiments.....	24
4.2 Image Acquisition and Analysis.....	27
4.3 Phase Behaviour Study.....	33
4.4 Interfacial Tension.....	34
<u>Chapter 5</u> Results and Discussion.....	35
5.1 Water Flooding.....	36
5.2 Alkaline Flooding.....	42
5.3 Flooding Experiments at Reservoir Temperature.....	57
5.4 Phase Behaviour.....	60
5.5 Interfacial Tension.....	70
<u>Chapter 6</u> Conclusion.....	75
6.1 Summary.....	75
6.2 Future Work.....	76
<u>Chapter 7</u> References.....	77
List of Figures.....	79
List of Tables.....	81

Abbreviations

AF	Alkaline flooding
ASP	Alkaline surfactant polymer
CDC	Capillary desaturation curve
DW	Deionized water
HC	Hydrocarbon
IFT	Interfacial tension
ME	Microemulsion
OIIP	Oil initially in place
OIP	Oil in place
O/W	Oil in water
PB	Phase behaviour
PV	Pore volume
RF	Recovery Factor
RPM	Rotations per minute
SW	Synthetic water
TAN	Total acid number
TDS	Total dissolved solids
TIS	Total ionic strength
WBT	Water break through
WF	Water flooding
W/O	Water in oil

Chapter 1

Introduction

Energy demand from hydrocarbon recovery will continue over the next couple of decades (International Energy Agency, 2018).

The recovery operations of hydrocarbons (HC) are divided into three stages, depending on the maturity of the field. HC production normally begins with natural depletion of the field (primary HC recovery) due to the initial pressure in the reservoir. As secondary HC recovery, the pressure of the reservoir is maintained by gas or water injection. If a reservoir is further depleted, enhanced oil recovery (EOR) methods can be applied (tertiary recovery). There are many different EOR methods published which were evaluated by the industry. However, there is no possible recovery method that will fit just any reservoir. Therefore, it is recommended to carefully select the most efficient recovery method for the given reservoir condition (EOR screening). Chemical flooding operations can mobilize trapped residual oil by lowering interfacial tension (IFT) as well as alter wettability condition in the case of alkaline or surfactant flooding and enhance water viscosity when using polymers.

This thesis focuses on investigating effects of alkaline flooding in microfluidics under ambient and reservoir temperature conditions.

1.1 Background and Context

This work follows the recent achievements of alkaline flooding in microfluidic experiments by (Borji, 2017) and (Kharrat, 2018) and phase behaviour studies as well as interfacial tension experiments from (Arnold, 2018).

1.2 Scope and Objectives

Alkaline flooding is applied with deionized water as well as a synthetic brine and compared at different concentrations. Furthermore, there are selected flooding scenarios which were carried out under reservoir temperature conditions. This allows a direct comparison of dynamic (microfluidics) and static (phase behaviour experiments) effects performed at both, ambient and reservoir temperature conditions.

The main objective of the present thesis is to reproduce earlier results and further to perform a combined study of static and dynamic effects at ambient and reservoir conditions.

Chapter 2

Literature Review

This chapter briefly introduces enhanced oil recovery with focus on chemical flooding and specifically on alkaline flooding.

2.1 Enhanced Oil Recovery

Generally, oil recovery is divided into three terms that describe different stages of the production of a reservoir or field, as follows: Primary recovery describes the oil recovery by natural drive mechanisms such as solution gas drive, gas cap drive, water influx due to an aquifer or gravity drainage. Secondary recovery refers to any methods that are applied in order to maintain the reservoir pressure such as gas or water injection. Primary and secondary recovery is also referred to as conventional recovery. The average recovery of conventional recovery is around 35% which leaves a great amount of hydrocarbon (HC) trapped in the reservoir due to capillary forces which hold the oil in place. Producing these remaining trapped HCs is aimed in EOR applications. Tertiary recovery refers to any other oil recovery method that is applied after secondary recovery (Lake, 2014).

The definition of enhanced oil recovery (EOR) is oil recovery by injection of fluids which are not normally present in the reservoir. This covers many different agents and processes in various stages of the production life of a reservoir, mostly but not necessarily as tertiary recovery. There are three main categories of EOR; thermal, chemical (surfactant) or miscible (solvent) methods (Lake, 2014).

2.2 Chemical Flooding

Chemical flooding is one type of EOR processes and deals with the injection of chemical solutions with the aim of mobilizing residual oil. Typical chemical solutions are alkaline, surfactant and polymer solutions. Alkaline solutions and surfactants are applied to reduce

capillary forces in the reservoir while polymers increase the water viscosity and reduce viscous fingering and thus improve sweep efficiency (Sheng, 2014).

Surface active agents (surfactants) can either be directly injected or created in-situ through the injection of an alkaline solution. The injected alkaline solution reacts with acidic components of crude oil and forms surfactants which lowers the interfacial tension (IFT) between the oil and the brine phase (Lake, 2014). The underlying saponification reaction is shown in equation (2.1) below:



HA Pseudo-acid component

A^- Surfactant component.

When alkaline flooding is applied in combination with surfactant and polymer flooding (ASP flooding) the alkali can reduce adsorption to grain surfaces and increase the efficiency of the surfactant (Sheng, 2014).

Further mechanisms of alkaline flooding include emulsification with oil entrainment or entrapment and wettability alteration. Oil entrainment refers to oil being emulsified into and transported within the water phase which improves the displacement efficiency. Oil entrapment happens when emulsion clusters are bigger than the pore throats, hence blocking the flow paths and forcing fluid flow through unswept pores which increases sweep efficiency. (Sheng, 2014) Wettability may change from oil-wet to water-wet or vice versa. Relative permeability changes favourably if an oil-wet system becomes water-wet but changing from water-wet to oil-wet may result in connecting trapped residual oil phases and provide new flow paths for the oil phase (Sheng, 2011).

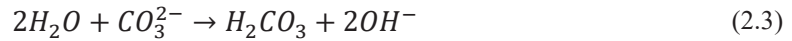
Some of the above-mentioned mechanisms were observed in the work of (Borji, 2017) and (Kharrat, 2018) as well as in this thesis.

The most commonly used chemicals for generating alkaline solutions are sodium carbonate (Na_2CO_3) and sodium hydroxide (NaOH) (Lake, 2014). There have been difficulties in breaking the emulsion when using a strong alkaline salt such as NaOH (Li, et al., 2005). To reduce emulsion and scale problems, all experiments in this thesis were performed using sodium carbonate as alkaline salt and the according reactions can be formulated as follows in equation (2.2) and (2.3) below.

First sodium carbonate dissociates in aqueous solution:



Through proton transfer hydroxide ions are produced and carbonic acid is formed:



The surfactants (A^- in equation (2.1)) lead to a great reduction in IFT. As a result, typically the capillary number is increased, emulsion phases may form, and wettability is altered (Gong, et al., 2016). The latter is not the main focus of this thesis since wettability changes are strongly dependent on the rock composition.

The capillary number (N_c) is the ratio of viscous to capillary forces which results in a dimensionless number. It is proportionally related to the IFT and its simplest definition is stated in equation (2.4) below.

$$N_c = \frac{\mu v}{\gamma} \quad (2.4)$$

- μ fluid viscosity [Pas]
 v velocity of displacing fluid [m/s]
 γ interfacial tension (IFT) [N/m]

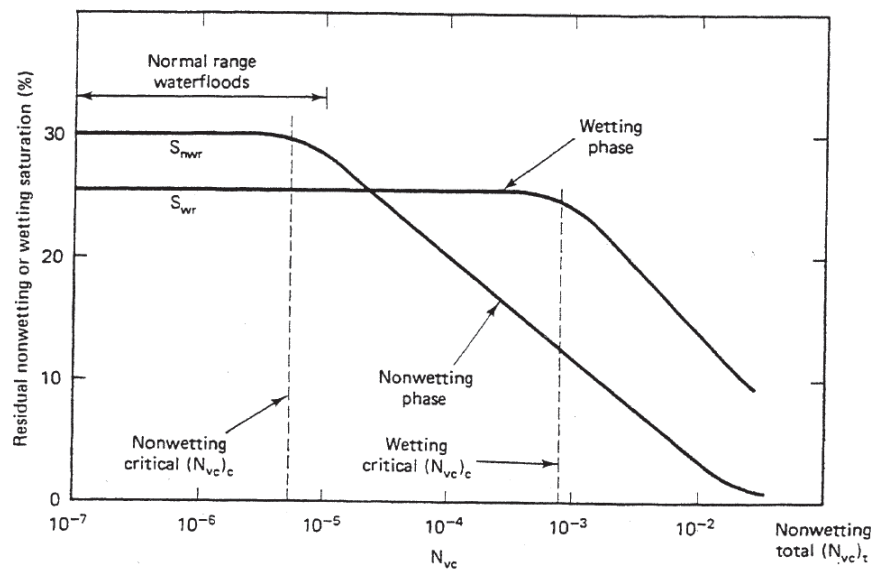


Figure 2.1 - Schematic Capillary Desaturation Curve (CDC) (Lake, 2014)

With decreasing IFT the capillary number increases and allows for a smaller residual oil saturation which is a target of EOR. Figure 2.1 above shows a schematic capillary desaturation curve (CDC) in which the relationship between the residual saturation and the capillary number is shown for each wetting and non-wetting fluid in a porous medium. For small capillary numbers, the residual saturation of the nonwetting fluid is constant at a plateau value. The constant plateau value of the residual saturation of the wetting fluid is lower and remains constant for a bigger range of capillary numbers. The critical capillary numbers for the nonwetting as well as wetting phase are the capillary numbers at which the respective residual saturation starts decreasing. This is where the reduction of a phase saturation starts. Hence,

desaturation of the nonwetting phase starts at smaller capillary numbers than for the wetting phase.

When N_c was compared to experimental data, the residual trapped nonwetting phase mobilization occurred around the value 10^{-6} (Dullien, 1979) which unfortunately are nonpredictive results because mobilization would be expected at a ratio of viscous to capillary forces of 1. Equation (2.4) assumes that viscous and capillary forces act on the same length scale which induces this inconsistency (Armstrong, et al., 2014). A new capillary number (2.5) was introduced by (Armstrong, et al., 2014), which may be applied for the interpretation of the oil distribution on a microscopic scale:

$$N_c^{macro} = \frac{-l^{cl}\mu_w v_D}{k_{rw}P_c} \quad (2.5)$$

N_c^{macro}	capillary number []
l^{cl}	cluster length [m]
μ_w	wetting phase viscosity [Pas]
v_D	Darcy velocity [m/s]
k_{rw}	relative permeability of the wetting phase [m ²]
P_c	capillary pressure [Pa]

Average values of the parameters in equation (2.5) were measured in fast X-ray computed microtomography and transformed to macro scale. Mobilization of the nonwetting phase was observed at $N_c^{macro} \sim 1$ (Armstrong, et al., 2014).

2.3 Phase Behaviour

The phase behaviour study is a fundamental test to get an understanding of the complex behaviour that different phases will establish when exposed to each other. A major parameter that influences phase behaviour is the salinity of the brine. In an ideal case, low salinity brines generally provide a good solubility for anionic surfactants, with an increasing salinity oil solubility is establishing. Winsor was one of the first to study and discover different phase behaviour characteristics.

The most common labels that describe emulsion formation are Winsor Type I, Type II, Type III, or Type II(-), Type II(+) and Type III respectively. Phase behaviour can easily be visualized and calculated in ternary diagrams (Figure 2.2). The labels Type II(-) and Type II(+) refer to two present phases and the negative or positive slope in the ternary diagram and the salinity of

the brine. Electrostatic forces decrease the surfactant solubility in high salinity water. The diagrams in Figure 2.2 show an ideal behaviour for pseudocomponents.

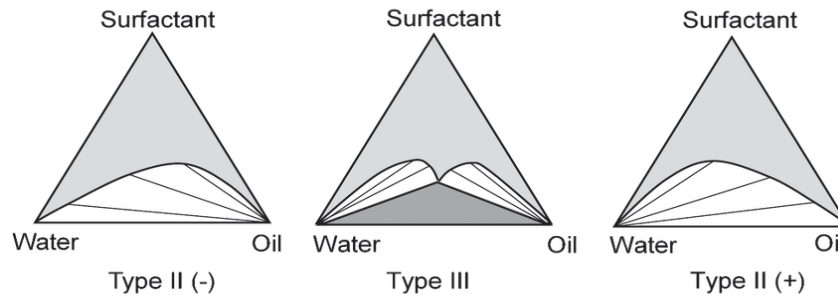


Figure 2.2 - Ternary diagram for Winsor types II and III.

From left to right (low salinity to high salinity water phase): Type II(-) (Type I) represents oil dissolved in the aqueous phase (O/W), Type III a three-phase system with a separate oil and water phase and a stable microemulsion (ME) phase between them, and Type II(+) (Type II) represents water dissolved in the oleic phase (W/O) (Lake, 2014).

Generally, a typical surfactant will exhibit poor oil-phase and good aqueous-phase solubility at low water salinity and vice versa at high water salinity. The phase in which solubility is poor will have a certain amount in excess which will remain in its pure form.

In alkaline flooding, the surfactants are generated in-situ when the alkali solution encounters the oil present in the reservoir. Phase behaviour is sensitive to many parameters and the fact that every crude oil composition is unique adds to the complexity.

The phase behaviour tests which are carried out in this thesis expose a complex crude oil to various solutions at different salinities. Therefore, emulsions of every kind (O/W), (W/O) and possibly microemulsions are to be expected. It is possible for several emulsion types to coexist in a real system.

Chapter 3

Experimental Devices and Equipment

This Chapter describes all used equipment and materials for conducting the experiments.

3.1 Micromodel and Microscope

For all microfluidic experiments performed in this thesis an EOR microfluidic chip manufactured by Micronit Microtechnologies was used. The chip is made of borosilicate glass and has a low thermal expansion coefficient.

There are different network types available such as a uniform network, random network or a physical pore rock network. The latter was used for all experiments and put into a high-pressure and high-temperature chip holder which is made of stainless steel. This combination has a maximum operation Temperature of 80°C and an operating pressure of 100bar. (Micronit, 2019)

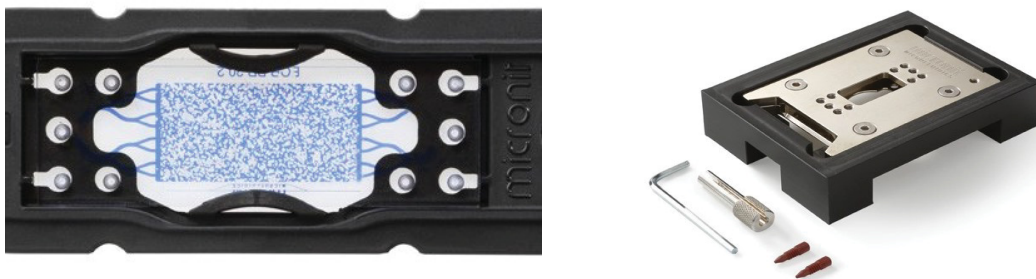


Figure 3.1 - Left: Physical Rock Model Right: Chip holder (Micronit, 2019)

This model and chip holder combination has one in- or outlet on each side and they were connected to tubing for fluid injection and production. The inlet was connected to a three-way valve, one flow line connecting to the syringe for injection which created a constant flow rate boundary during the experiments and the other line which ended in atmospheric conditions to de-air the system when changing the injection syringes and fluids. The outlet tube had a simple

valve attached which was connected to a waste vessel at atmospheric conditions creating a constant pressure boundary during the flooding experiments. Prior to oil saturation, this valve was attached to a vacuum flow line to evacuate flow lines and the micromodel.

Table 3.1 - Physical Rock Network Specifications (Micronit, 2019)

Porosity [%]	Permeability [D]	PV [μl]	Distance of channel to top surface [μm]	Distance of channel to bottom surface [μm]
57	2.5	2.3	1100	680

The chip holder was placed on the wide-range automated table (moving stage) of a high-end microscope (DMi 8) from Leica. Images were recorded by a Leica camera (DMC2900) from below. The automatic image stitching option, providing a high spatial and time resolution, was used and allowed to closely investigate the displacement processes.

3.2 Temperature Setup

For experiments at ambient temperature conditions, a light source from above was used to illuminate the micromodel. Experiments at reservoir temperature conditions were carried out by placing a metal block which was heated by an electric circuit (with a proportional-integral-derivative (PID) controller) on top of the micromodel. This setup required the usage of the bottom light source as depicted in Figure 3.2.

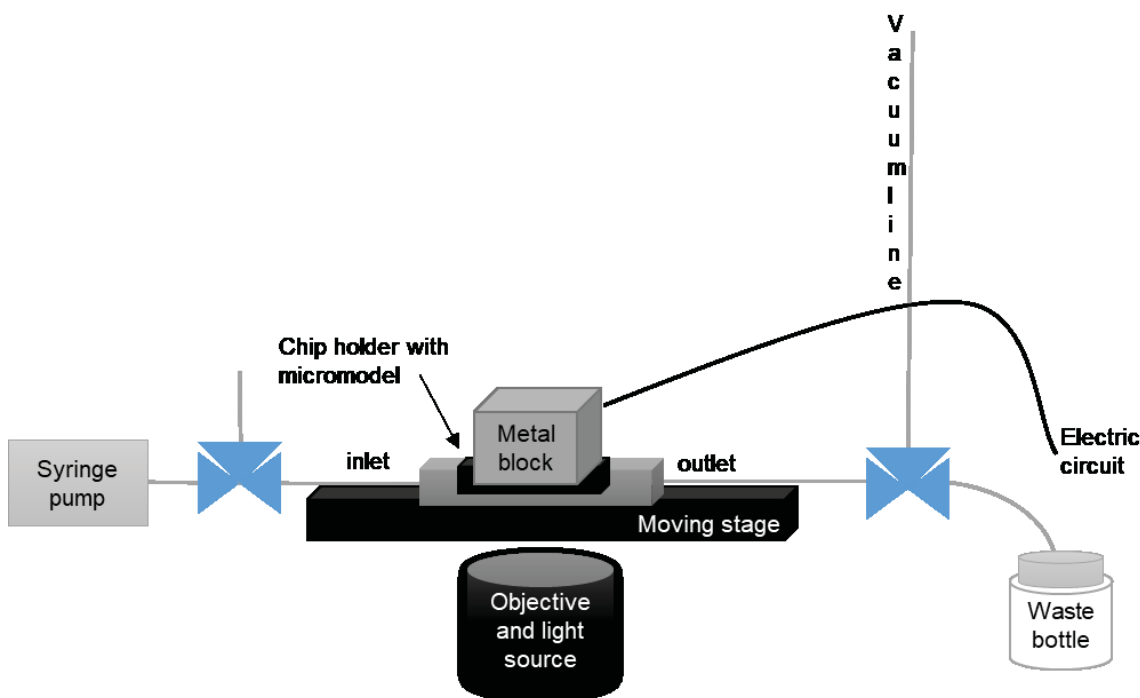


Figure 3.2 - Schematic Experimental Setup

The metal block and electric circuit were provided by colleagues from the university's Department of Electrical Engineering (Institut für Elektrotechnik, Montanuniversität Leoben) as a quick and temporary heating solution. A thermal conductive pad was attached to the metal block to achieve an even temperature distribution in the micromodel. The metal block did not completely fit in the cavity of the chip holder (2cm x1cm) but covered the area of the porous medium itself. Thermal grease was applied to the entire glass surface area to help distribute temperature and isolate the small area around the contact area to the metal block. The temperature of the metal block was regulated by using the PID controller and measured with a contact thermometer.

3.3 Injection Equipment

For injection purposes, a high precision syringe pump (model Fusion 200 from Chemyx Inc.) was used. Syringe pumps are more convenient for injection purposes than piston pumps because small particles, that are present in crude oil, would settle down in the piston pump (Kharrat, 2018). At low flow rates, syringe pumps show a higher oscillation of pressure compared to piston pumps. Plastic syringes however, enhance pressure stability and therefore reduce the pulsation compared to glass syringes. The instability can be further reduced by using smaller diameter syringes in order to achieve a more continuous piston movement. The best way could be to use the syringe pump for saturating the model with oil and then change to a pulse free piston pump for injecting the displacing fluids for the experiment although this pump is much more complicated to set up and clean (Borji, 2017).

For the microfluidic experiments in this work, a plastic syringe from B Braun of 10ml with an inner diameter of 15.96mm was used to achieve the same conditions and produce comparable data to the work of colleagues at the Department of Reservoir Engineering.

For cleaning purposes, a gas tight glass syringe from Hamilton of 5ml with an inner diameter of 10.30mm was used additionally. Furthermore, there was a microfluidic tubing with a filter available for cleaning purposes to avoid dust particles from entering the micromodel.

3.4 Additional Equipment

For weighing purposes, a precision balance (model EG 220-3NM from KERN) was used. The Hei-Mix S magnetic mixer from Heidolph was utilized to mix salts with distilled water and produce different brine and alkaline concentrations. These fluids were stored in glass bottles. A rack with test tubes (BRAND) of 10ml was used to carry out phase behaviour experiments. The phase behaviour experiments were heated in an oven.

IFT measurements were carried out using a spinning drop setup (SVT 20N from Dataphysics in combination with their SVT20 software) which was explained in detail in the research of (Arnold, 2018).

Chapter 4

Methodology

All experiments in this thesis were performed with the same crude oil. Some properties of this oil are listed in Table 4.1 below.

Table 4.1 - Oil properties

TAN [mgKOH/g oil]	Density at 20°C [g/cm ³]	Viscosity at 20°C [cp]	°API
1.56	0.9070	80	23.79

A synthetic brine (SW), as well as different alkali solutions with either deionized water (DW) or SW, were prepared synthetically in the lab, each in 250ml badges. The water density value at an ambient temperature of 23°C is 0.99753g/cm³ ⁽¹⁾ and was used to calculate the according weight. The salts sodium chloride (NaCl), sodium bicarbonate (NaHCO₃) and sodium carbonate (Na₂CO₃) from the company Sigma Aldrich were used in the process of mixing brine and alkaline solutions. The total dissolved solids (TDS) in the SW were 20.81g/l.

Table 4.2 – Synthetic Brine (SW) Composition

H2O [g]	NaCl [g]	NaHCO ₃ [g]
249.38	4.74	0.4625

For the alkali flooding experiments sodium carbonate was added to DW and SW. A total of 6 different mixtures were prepared as stated in Table 4.3.

Table 4.3 - Prepared Injection Fluids

Water	Alkali concentration (Na ₂ CO ₃) [ppm]	TDS [g/l]	TIS [mol/l]
DW	0	0	0
DW	3000	3	0.0849
SW	0	20.81	0.346
SW	200	21.01	0.352
SW	1000	21.81	0.375
SW	3000	23.81	0.431
SW	5000	25.81	0.488
SW	12000	32.81	0.686

The total ionic strength (TIS) was calculated as stated in equation (4.1).

$$TIS = \frac{1}{2} \sum_i c_i z_i^2 \quad (4.1)$$

i ion in solution []

c_i concentration of i [mol/l]

z_i charge of i []

4.1 Microfluidic Experiments

The clean micromodel was connected to the vacuum pump at its outlet valve (the inlet valve remained closed) and vacuumed for 1.5 hours. Meanwhile, a few ml of crude oil was poured into a small beaker and drawn up into the plastic syringe. The syringe filled with oil was mounted on the syringe pump and connected to the inlet valve. The pump was set to start at 10ml/h to remove all air in the tube and valve. The rate was then gradually set back to 1ml/h and after 10 minutes at the target rate, the inlet valve was opened to saturate the microchip.

Figure 4.1 shows the fully oil saturated micromodel. The pore space filled with oil is grey and white areas depict the grains of this 2D porous medium.

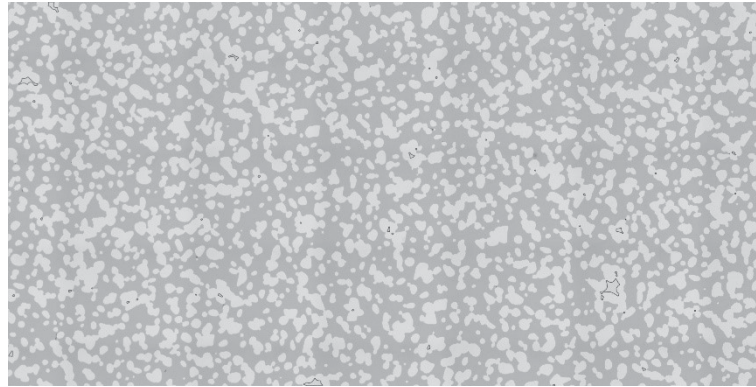


Figure 4.1 – Oil Saturated Micromodel

Once the microchip was fully saturated, the injection rate was gradually set back (bisect the rate every 10 minutes) to the target injection rate of 0.002ml/h to produce comparable results to past and future work of other colleagues in this department. This approximately relates to an injection rate of 1 ft/day.

After the target injection rate was reached the inlet valve was closed and connected with the tubes and syringe for water flooding. Separate tubes were used for oil saturation and water/alkaline flooding since the water might not be able to properly clean out the oil inside the tube and oil might temporarily be bypassed and later be reinjected during water or alkaline flooding. The injection rate was once again set to 10ml/h to remove air in the tube and oil in the valve and then gradually (in the same manner as explained before) set back to the target rate at which the valve was opened. This process was carried out the same way when the water flooding finished and changed to alkaline flooding.

Table 4.4 gives an overview of all experiments that were carried out on the micromodel.

Table 4.4 - Overview Microfluidic Experiments

Experiment	Water flooding	Alkaline flooding	Temperature
Exp. 1	SW	-	23°C
Exp. 2	SW	SW with 200ppm Na ₂ CO ₃	23°C
Exp. 3	SW	SW with 1000ppm Na ₂ CO ₃	23°C
Exp. 4	SW	SW with 3000ppm Na ₂ CO ₃	23°C

Exp. 5	DW	DW with 3000ppm Na ₂ CO ₃	23°C
Exp. 6	SW	DW with 3000ppm Na ₂ CO ₃	23°C
Exp. 7	SW	DW with 3000ppm Na ₂ CO ₃	23°C
Exp. 8	SW	DW with 3000ppm Na ₂ CO ₃	50°C
Exp. 9	SW	DW with 3000ppm Na ₂ CO ₃	60°C
Exp. 10	SW	SW with 3000ppm Na ₂ CO ₃	60°C
Exp. 11	SW	DW with 3000ppm Na ₂ CO ₃	60°C
Exp. 12	SW	SW with 5000ppm Na ₂ CO ₃	23°C
Exp. 13	SW	SW with 12000ppm Na ₂ CO ₃	23°C

After experiment 10 a new micromodel was used since the one used so far was damaged in the process of re-assembling. Some experiments were repeated and will further be discussed in chapter 5. For simplicity, the alkaline fluids will from now on be referred to in abbreviations, e.g. SW3000 refers to synthetic water (SW) with 3000ppm of Na₂CO₃.

4.1.1 Cleaning Procedure

In order to ensure the same initial conditions for each microfluidic experiment, the micromodel was systematically cleaned before all experiments as follows:

The following procedure suggested by (Kharrat, 2018), based on (Borji, 2017), was initially followed:

1. Rinse with 1.5-2ml Acetone at 10ml/h to remove water and partly react with oil but not for a long time that may cause change in wettability.
2. Flood with approximately 2ml Toluene at 0.3 to 0.5ml/h for at least 4 hours, depending on the severity of contamination to ensure that all traces of oil are removed.
3. Rinse with 1.5-2ml Acetone at 10 ml/h.
4. Dry by injecting air (2ml at 10ml/h) and evaporate the acetone completely.
5. Vacuum at least 1.5 hours before saturating with oil.

Acetone and Toluene were injected through a filter to minimize contamination of the micromodel.

Crude oil often contains particles which can enter and accumulate in the micromodel with each oil saturation. Residual traces of oil and emulsion phases were more difficult to remove as the alkali concentration increased. After the fifth experiment, the cleaning procedure had to be adjusted to become more effective. Before each new experiment, the micromodel was visually checked to ensure it is in a clean state and has no traces of oil left. When there were traces of salt left, the model was flushed with distilled water before the cleaning procedure. Then, if a significant amount of oil was left, decane (95%) was used to bind and remove remaining oil. For some experiments, the cleaning procedure was repeated a second time and for a couple of minutes, a higher pressure was used during the acetone flush. The outlet was closed for 2-5 minutes to build up pressure and reach narrow pores which are not easily accessible in flow direction. When closing the outlet valve the model was supervised constantly to track the fluid movement through those problematic pores. Additionally, the cleaning procedure was once carried out against flow direction (after Exp. 6) which helped removing traces of oil in badly accessible parts of the model.

4.2 Image Acquisition and Analysis

The Leica microscope was used with a magnification of 2.5x and a field of view of 3742 μm times 2806 μm which resulted in 34 image tiles that were automatically stitched together by the Leica X software. Experiments at ambient temperatures were recorded with usage of the top light. (light source from top). Images of experiments at reservoir temperature were recorded using the fluorescent light and filter cubes to achieve a desirable contrast (Figure 4.2). In this case grains as well as water were black and oil was orange.

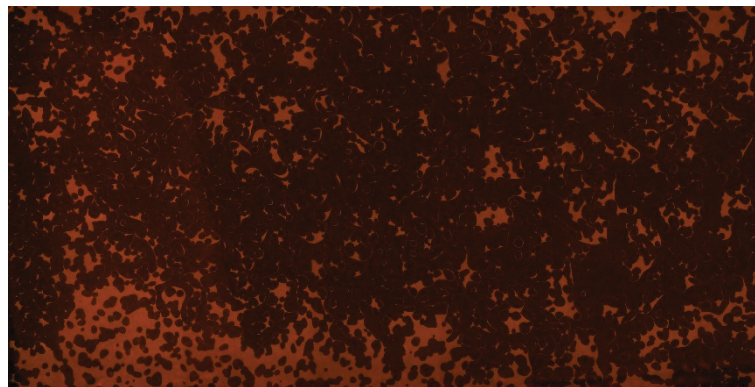


Figure 4.2 – Colour picture of fluorescent light modus during a waterflooding experiment

All image analysis was carried out by using the software package Fiji from ImageJ. The procedure of (Kharrat, 2018) and (Borji, 2017) was followed and after rotating and cropping each experiment image series individually, the same steps were repeated for all images which included binarizing and first eroding and then diluting each image the same amount of times, to get rid of black pixels at the grain surfaces and inside grains (Figure 4.3) since oil is represented by black pixels and grains and water are both white pixels in the binarized pictures.

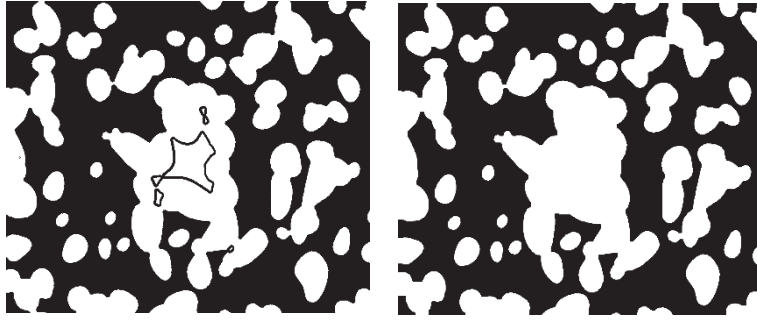


Figure 4.3 – Binarized outcrop of the oil saturated micromodel.

Left: before the image was eroded; right: after the image was eroded and diluted

4.2.1 Recovery Factor

The water flooding experiments (SW or DW) were the primary applied recovery method, however, the recovery after water flooding was referred to as secondary recovery. The software ImageJ measured the number of black pixels which was then used to calculate the secondary recovery factor:

$$RF(secondary) = \left(1 - \frac{OIP_w}{OIIP}\right) \quad (4.2)$$

where OIP_w is OIP after water flooding and $OIIP$ is oil initially in place.

The tertiary recovery refers to the additional recovery that was reached after each alkali injection compared to the brine (SW) or deionized water (DW) injection beforehand:

$$RF(tertiary) = \left(1 - \frac{OIP_a}{OIP_w}\right) \quad (4.3)$$

where OIP_a is OIP after alkaline flooding and OIP_w is OIP after water flooding.

The ultimate recovery is the recovery that was reached at the end of alkaline flooding:

$$RF = \left(1 - \frac{OIP_a}{OIIP}\right) \quad (4.4)$$

where OIP_a is OIP after alkaline flooding and $OIIP$ is oil initially in place.

4.2.2 Cluster Volume and Lorenz analysis

The idea was to investigate and compare the areas in which oil remained after each water and alkaline flooding experiment. Typically, residual oil remains within clusters or droplets of different sizes. If the porous medium is oil wetting (as it initially is, since the porous medium is 100% oil saturated), the oil will remain in clusters around grains. When the porous medium changes to mixed-wet conditions which happens during water and alkaline flooding, the oil will form droplets which then can get stuck in pore channels and become residual oil (Kharrat, 2018).

At a certain linear behaviour of frequency of clusters to volume of clusters, the capillary number will be one. Values below that linear relationship suggest that the oil volume is dictated by small clusters, values above that relationship suggest that the oil volume is dictated by large clusters. The IFT is reduced during alkaline flooding which can directly be translated to that linear relationship shifting towards the smaller clusters which are more difficult to recover.

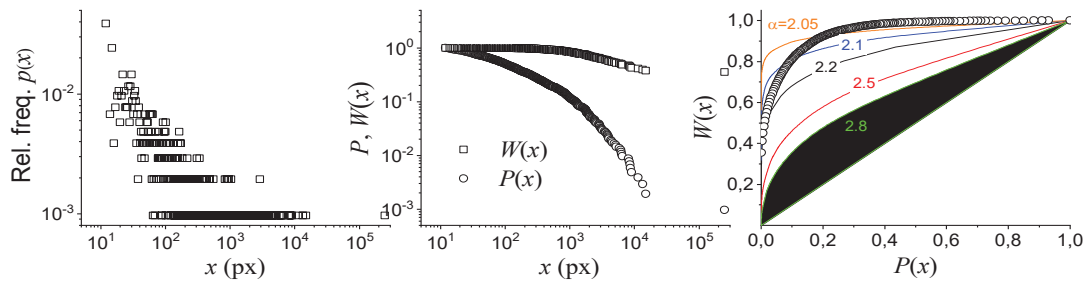


Figure 4.4 – Cluster Volume and Lorenz Analysis.

These figures show data from a water flooding experiment. The plot on the left shows a cluster volume distribution (the relative frequency of clusters as a function of their size). In the middle the cluster size is plotted in relation to the cumulative cluster volume distribution ($P(x)$) and the volume weighted cumulative cluster volume distribution ($W(x)$). The right plot shows the Lorenz plot (relationship between $W(x)$ and $P(x)$) where the diagonal line represents a homogeneous distribution between oil volume and cluster size). The area underneath the curves is a measure of “heterogeneity”. For fractal distributions: $W = P^{(\alpha-2)/(\alpha-1)}$ (Ott, et al., 2019).

Empirical data from experiments typically show a wide range of observed cluster volumes (Kharrat, 2018). To remove this scatter (left plot in Figure 4.4) and normalize the data the following integration (4.5) was applied:

$$P(x) = \int_x^{\infty} p(y) dy \quad (4.5)$$

A MATLAB code by (Clauset, et al., 2009) based on equation (4.5) was applied to calculate the cumulative cluster size distribution and fit it to the power law maximum likelihood function.

The upper plot in Figure 4.5 shows curves for brine and alkaline flooding after applying the power law equation (PL) to normalize the distribution of cluster volumes. $P(x)$ gives the fraction

of a cluster based on its volume, the volume of clusters is displayed in pixels. The brine and alkaline flooding curves typically differ from each other as the clusters get bigger (cluster volume increases). This shows that after alkaline flooding there exist fewer big clusters compared to brine flooding.

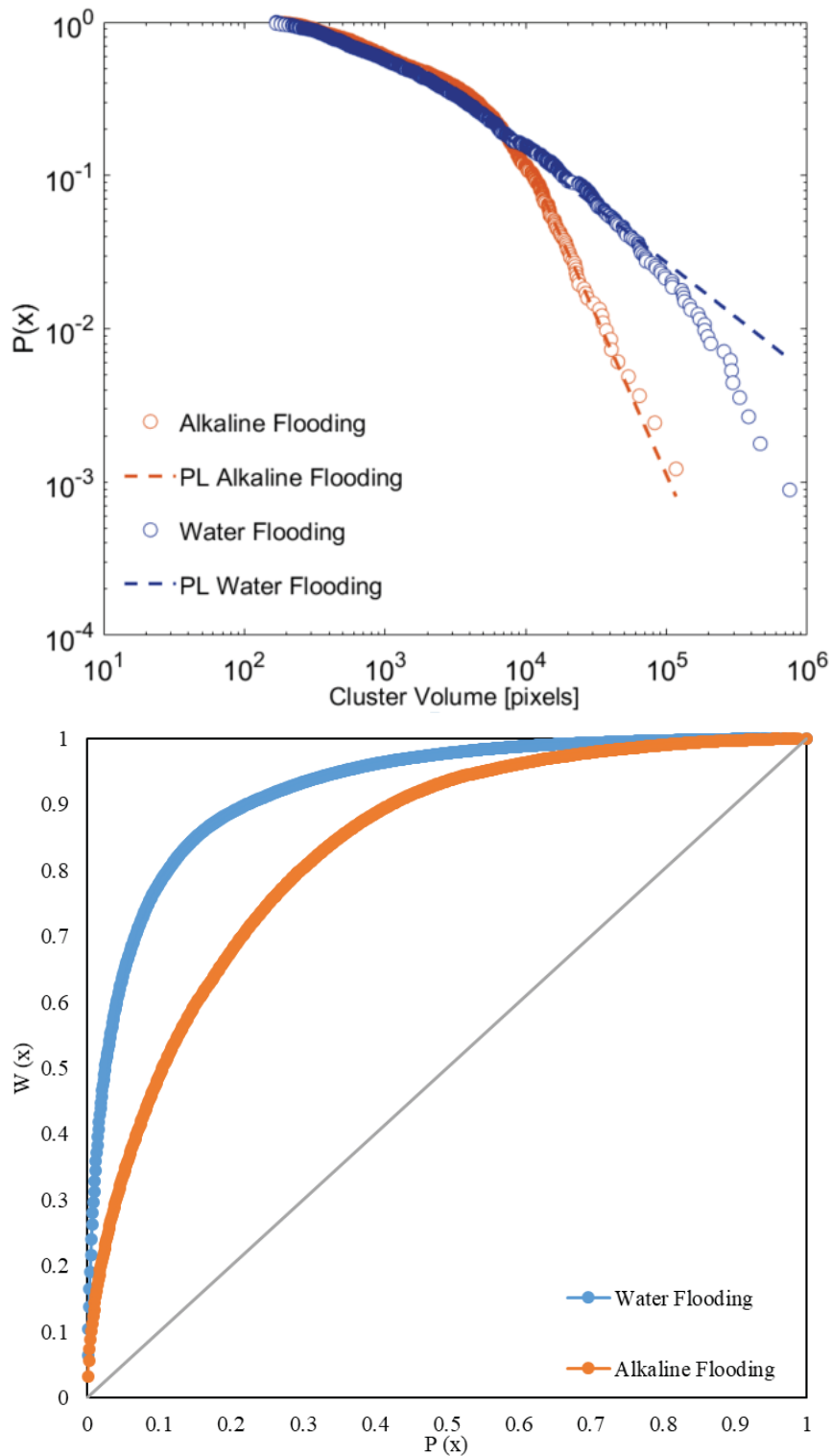


Figure 4.5 – Example “Cluster Analysis” plot (top) and example Lorenz Plot (bottom).

Furthermore, the Lorenz curve analysis can be applied and help visualize the cluster size distribution which was first done by (Kharrat, 2018). A volume weighted cumulative cluster size distribution, $W(x)$ was introduced:

$$W(x) = \frac{\int_x^{\infty} y p(y) dy}{\int_{x_{min}}^{\infty} y p(y) dy} \quad (4.6)$$

The lower plot in Figure 4.5 shows the Lorenz plot with $P(x)$ as the fraction of clusters based on size and $W(x)$ as the fraction of total oil volume inside the clusters.

The DW water flood (blue curve) is furthest in the left upper corner which shows high EOR potential because a large volume of oil is sitting in a very small fraction (amount) of clusters and they are considered to be easier to mobilize or break up by viscous forces. The orange curve (from the DW with 3000ppm alkaline flood) shows significantly less residual oil in big clusters. The grey line represents a homogeneous distribution of oil volume to cluster sizes as described before in Figure 4.4.

The area between the curves of water flooding and alkaline flooding in the Lorenz plot was calculated as stated in equation (4.7).

$$\Delta L = \int_0^1 (W(x)_{WF} - W(x)_{AF}) \quad (4.7)$$

where ΔL is the difference in Lorenz curves, $W(x)_{WF}$ is $W(x)$ after water flooding and $W(x)_{AF}$ is $W(x)$ after alkaline flooding.

4.2.3 Euler Characteristic

As briefly mentioned before it is expected that the wettability of the porous medium changes during the different flooding stages. The system starts out as completely oil wet (100% saturated with oil) and during water flooding oil is partially displaced by water. During water

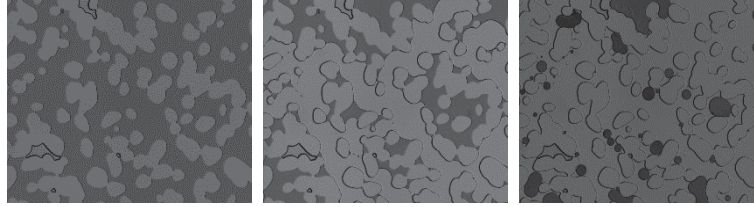


Figure 4.6 – Sub volumes of the micromodel at different stages of flooding experiments.

Left to right: oil saturated, after water flooding, after alkaline flooding

flooding some grain surfaces might become water-wet, however, mostly a lot of grains remain covered by oil clusters around them, therefore, the porous space is considered to be a mixed-wet system. During alkaline flooding, these oil clusters typically break up due to viscous forces and form smaller droplets which do not wet the grains, hence the porous space is becoming a water-wet system.

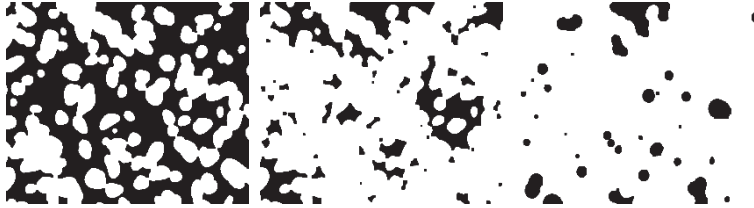


Figure 4.7 - Binarized images of Figure 4.6

(Armstrong, et al., 2018) linked the wetting state to the Euler characteristic (χ) which describes the fluid connectivity. In a 2D case the Euler characteristic can be calculated as shown in equation (4.8).

$$\chi = \beta_0 - \beta_1 \quad (4.8)$$

where β_0 is the number of objects and β_1 is the number of holes in the structure.

In order to have a direct relation to an oil volume of the cluster rather than only counting objects no matter their size (Ott, et al., 2019) introduced a normalized Euler characteristic χ_{vs} scaled by cluster volumes:

$$\chi_{vs} = \frac{\sum_{n_{cl}} V_{cl} \chi_{cl}}{\sum_{n_{cl}} V_{cl}} \quad (4.9)$$

where n_{cl} is the number, V_{cl} the volume and χ_{cl} the Euler number of an individual cluster.

If equation (4.9) is applied to the three segments in Figure 4.7, the oil saturated sub volume on the left results in a normalized Euler number of $\chi_{vs} = -24.8$, the water flooding sub volume in the middle results in $\chi_{vs} = 0.16$ and the alkaline flooding sub volume on the right in $\chi_{vs} = 1$.

A system with $\chi_{vs} < 0$ is referred to as an oil-wet system and $0 < \chi_{vs} < 1$ water-wet with $\chi_{vs} = 1$ being completely water-wet with only individual oil droplets.

4.3 Phase Behaviour Study

The phase behaviour study was carried out by filling 10ml test tubes with 5ml of each phase i.e. an aqueous and an oleic phase. The denser brine or alkali solutions (aqueous phase) was filled in first, then the oil was filled in on top. Then the tubes were closed with their joints and shaken well by hand (turbulent mixing condition). One set of test tubes was placed in a rack and left still for at least 72 hours to reach equilibrium at ambient temperature. Another set of test tubes was placed in the oven immediately after mixing, to reach equilibrium at reservoir temperature (60°C). The set that reached equilibrium at ambient temperature was later put in the oven at 60°C to investigate if the phase behaviour would shift under changing temperature conditions. Table 4.5 below shows all produced phase behaviour tests.

Table 4.5 - Overview Phase Behaviour Experiments

Brine/Alkali solution	Equilibrium at ambient temperature (23°C)	Equilibrium at reservoir temperature (60°C)
DW	x	x
DW3000	x	x
SW	x	x
SW200	x	
SW1000	x	
SW3000	x	x
SW4000		x
SW5000	x	x
SW6000		x
SW9000		x
SW12000	x	x

For the sake of simplicity, fluids which contain alkali are referred to in a short form: e.g. SW3000 is SW with 3000ppm Na_2CO_3 .

4.4 Interfacial Tension

Interfacial tension (IFT) data of oil with DW as well as oil in DW3000 was acquired directly from (Arnold, 2018). The IFT between the oil and SW as well as oil and SW3000 was measured in a spinning drop tensiometer (SVT 20N from Dataphysics) following the experimental procedure of (Arnold, 2018). Table 4.6 states the main input parameters for those spinning drop measurements.

Table 4.6 - Spinning Drop Input Parameters

Water density [g/cm ³] at 20°C	Oil density [g/cm ³] at 20°C	Target RPM	Magnification	Vertical Scale [pixel/mm]
0.998305	0.9070	3000	1.0x	134.32

Chapter 5

Results and Discussion

This chapter will list and discuss all acquired results and is addressing various challenges encountered throughout this work. It is divided into subchapters of water flooding, alkaline flooding, flooding experiments at reservoir temperature conditions, phase behaviour including a comparison of observed emulsion formation during flooding experiments and finally interfacial tension.

First, all resulting recovery factors (RF) and normalized Euler numbers are listed in Table 5.1 below, experiments which are marked with a “*” were repeated for some reasons:

Table 5.1 – Results: Recovery Factor and normalized Euler number

Name	Water flooding	Secondary RF [%]	Norm. Euler	Alkaline flooding	Tertiary RF [%]	Norm. Euler	Ultimate RF [%]
Exp. 1	SW	68.53	-3.45	-	-	-	68.53
Exp. 2	SW	73.20	-0.23	SW200	-2.08	-0.26	72.65
Exp. 3	SW	76.31	0.5	SW1000	-5.63	0.57	74.98
Exp. 4	SW	75.85	0.35	SW3000	-3.12	0.36	75.09
Exp. 5	DW	65.3	-0.83	DW3000	68.9	0.73	89.22
Exp. 6*	SW	66.12	-48	DW3000	17.18	-0.09	71.94
Exp. 7	SW	76.44	0.5	DW3000	11.52	-0.31	79.15
Exp. 8*	SW	-	-	DW3000	-	0.46	75.78
Exp. 9*	SW	-	-	DW3000	-	-29.75	59.18

Exp. 10	SW	70.08	-3.39	SW3000	-1.64	-0.38	70.6
Exp. 11	SW	65.84	-9.94	DW3000	16.82	-2.89	71.58
Exp. 12	SW	74.58	-8.97	SW5000	16.72	0.66	91.3
Exp. 13	SW	72.96	-4.67	SW12000	86.34	0.87	96.31

The water flooding result of Exp. 6* looked significantly different from previous experiments with SW flooding. This will further be discussed in the following chapter 5.1. Exp. 8* was repeated as Exp. 9* at 60°C but the image quality was not satisfying using the bottom light only, therefore it was repeated as Exp. 11 at 60°C using the fluorescent mode of the microscope. Experiments at reservoir temperature (60°C) will be further discussed in detail in chapter 5.3.

5.1 Water Flooding

The SW flooding scenarios resulted in secondary RFs around 70-75%. The displacement pattern, as well as the end state of water flooding, looked very similar for most SW experiments. The secondary RF did not change much after an injection of 1.5 PV. Therefore, all acquired data which allowed for time-dependent plots is shown until 1.5 PV injected in the figure below:

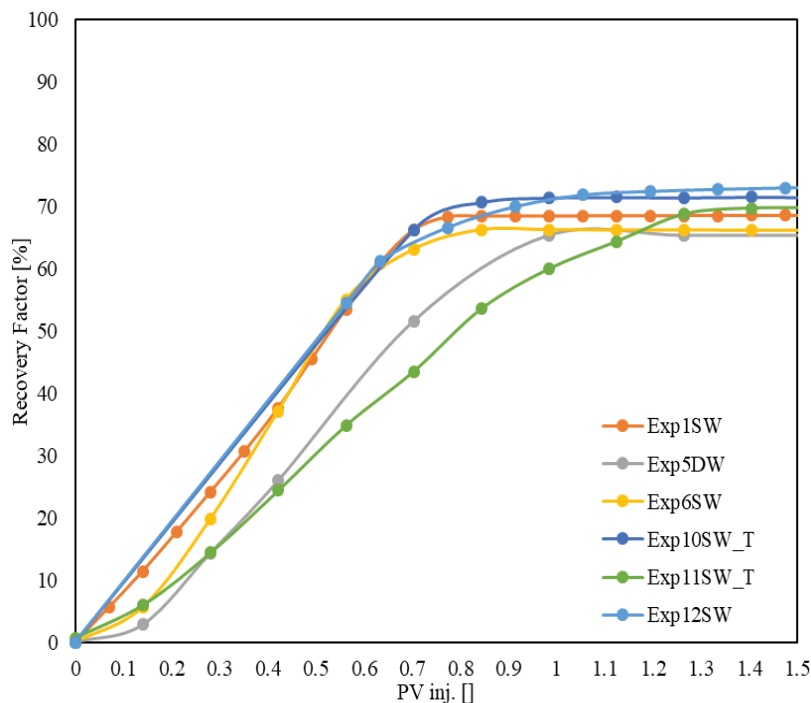


Figure 5.1 - Time dependent RF of water flooding scenarios.

Experiments which were carried out at reservoir temperature have an extended name (“_T”).

The water flooding front reached the inlet after 11-20 hours which is a very wide range of time and uncertainty and has to do with the volume of liquid in the inlet valve. Although the injection fluids were first injected at high pressure through the valve itself to displace remaining oil this apparently could not always be achieved in the same way. Remaining oil from the valve twice entered the model hours after a water flooding experiment had started. Those experiments were not further carried out and the cleaning procedure was repeated.

The average time until water break through (WBT) was 55 minutes (50 minutes to 1 hour with exception of Exp. 6 which reached WBT after 40 minutes).

Anomalous observations on selected SW flooding experiments

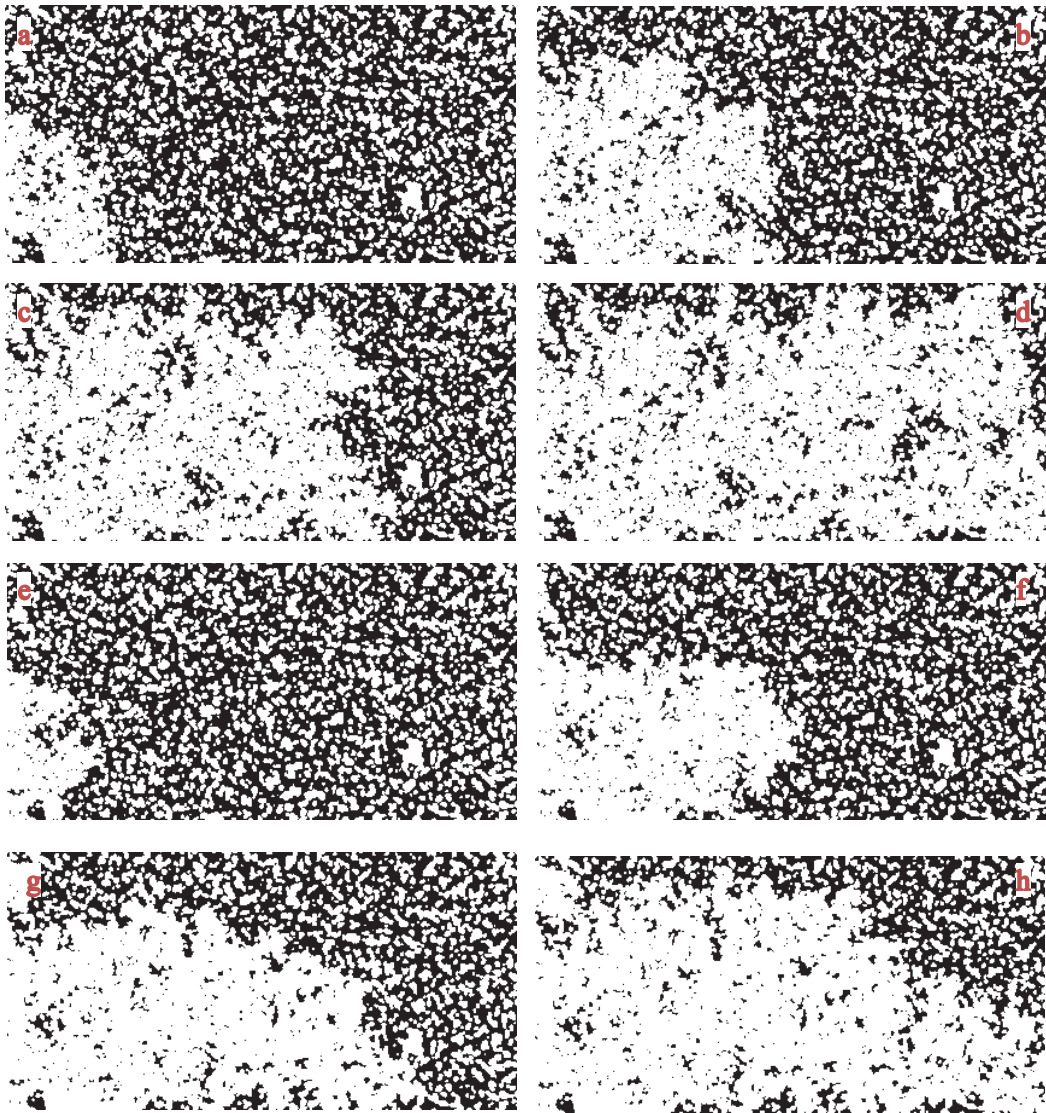
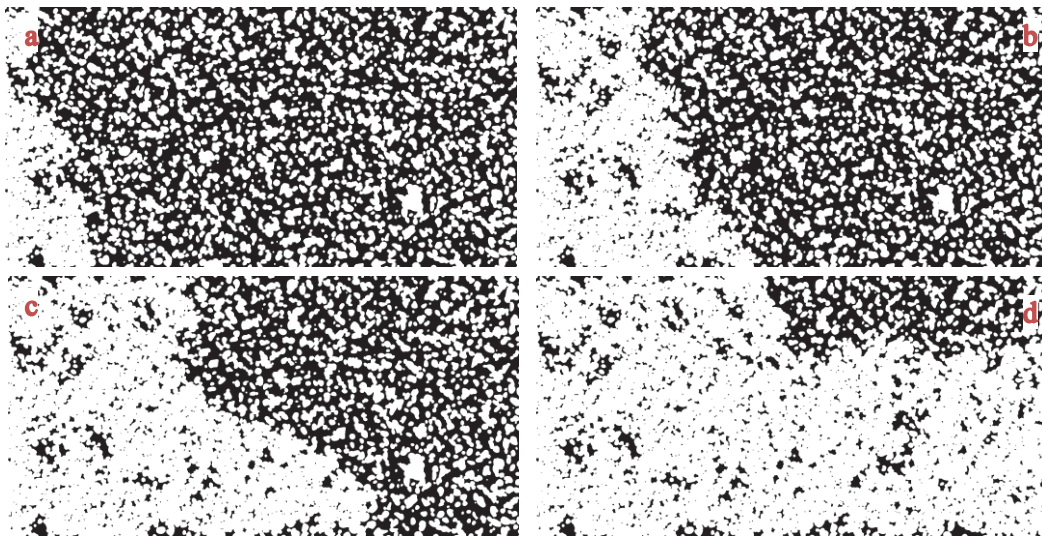


Figure 5.2 – Water flooding displacement patterns with a time interval of 20min. a)-d): Exp. 1 SW; e)-h): Exp. 11 SW. A general trend of the water front moving from the lower left corner to the upper right corner was visible in both experiments.

Exp. 1 and Exp. 11 were each the first experiments carried out on new micromodels. Both resulted in low secondary recovery factors compared to all other SW flooding experiments at ambient temperature conditions. Figure 5.2 shows the displacement pattern which was observed for Exp. 1 and Exp. 11. Although the same cleaning procedure and preparation was carried out before those experiments, they showed alternate flooding patterns compared to following experiments which might be a result of a slightly different initial wettability state compared to all following experiments.

Another experiment in which a possible issue with initial wettability conditions occurred was Exp. 6. This experiment started with a quite stable displacement front (images a and b in Figure 5.3) which was similarly observed during most of the other SW flooding experiments, but after 20 minutes (image c in Figure 5.3) the SW front already strongly differed from other experiments and the end state (image d in Figure 5.3) showed one big oil cluster remaining in the upper right part of the micromodel. WBT for this experiment occurred after 40 minutes. This happened exclusively for this experiment which therefore was repeated as Exp. 7. The alternate flow pattern has most likely formed due to an unsuccessful cleaning procedure beforehand.



*Figure 5.3 - SW anomalous displacement pattern in Exp. 6.
a) - c) 10 min interval and d) final state after water flooding*

Water flooding experiments at ambient temperature

Exp. 3 and Exp. 7 both showed a stable displacement front during water flooding, in a similar way as the initially stable front of Exp. 6 (image a in Figure 5.3). Figure 5.4 below shows the final states of SW flooding in Exp. 2, Exp. 3, Exp. 4 and Exp. 7.

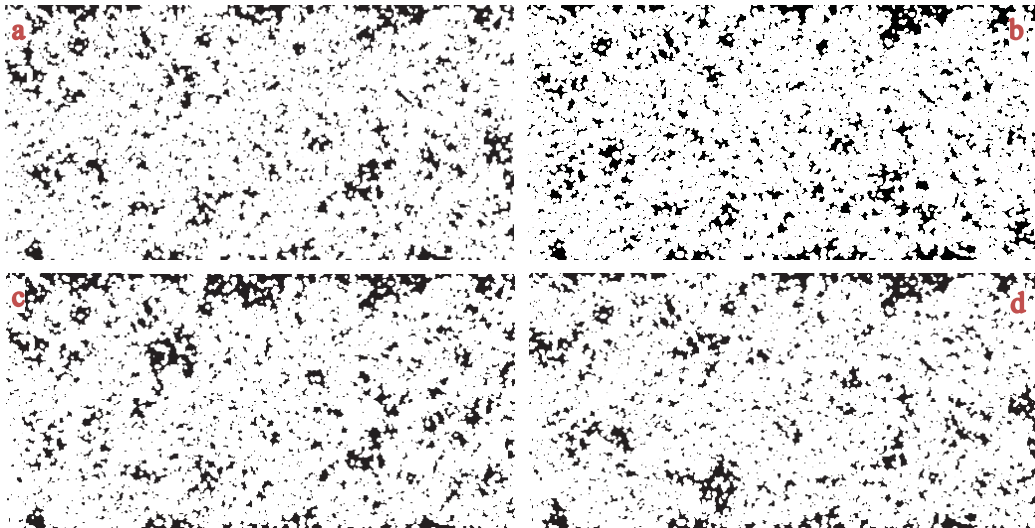


Figure 5.4 – Final states after water flooding with SW: a) Exp. 3, b) Exp. 7, c) Exp. 2, d) Exp. 4

From the binarized pictures, it might seem that Exp. 3 and Exp. 7 (images a and b in Figure 5.4) had many of the remaining oil clusters in the same areas, containing similar volumes. This would cohere with their almost same secondary RFs of 76.31% and 76.44% (Table 5.1) and identical normalized Euler number of 0.5, indicating that both reached a water-wet state during SW flooding. However, the Lorenz plot in Figure 5.5 suggests that Exp. 3 had a much greater EOR potential than Exp. 7, hence more oil was left in bigger clusters. The other three experiments in Figure 5.4 (Exp. 2, 4 and 7) showed a quite similar relationship of the cluster size and volume distribution (Figure 5.5). Exp. 4 resulted in a positive normalized Euler number of 0.35 and therefore had reached water-wet state while Exp. 2 with -0.23 would, per definition, still be considered oil-wet.

During all water flooding scenarios, the normalized Euler number strived towards a water-wet system, but this was only reached in Exp. 3, Exp. 4 and Exp. 7 due to the analysis.

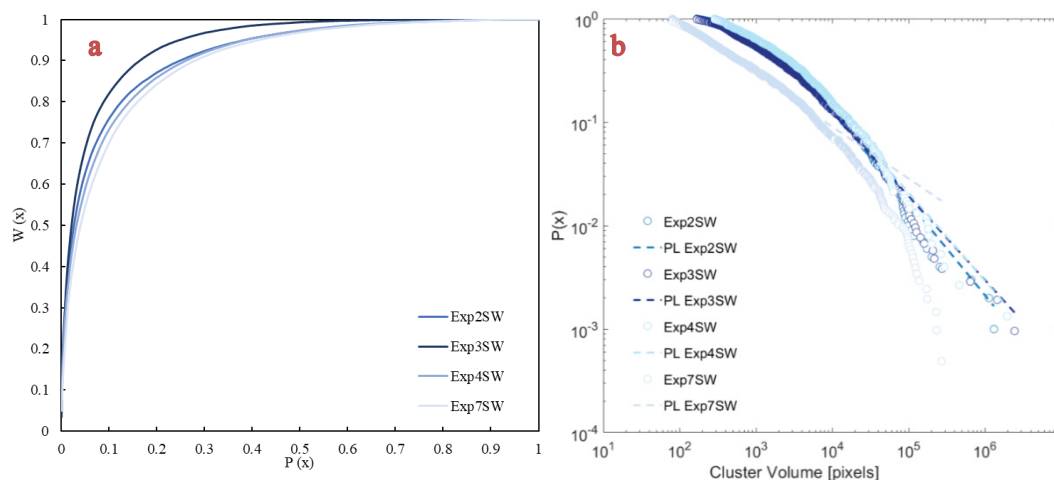


Figure 5.5 – SW flooding of Exp. 2, 3, 4 and 7 a) Lorenz Plot and b) Cluster Analysis

The DW flooding in Exp. 5 resulted in the lowest secondary RF. It was expected that the salinity of the SW would improve the water flooding compared to DW. The salt contained in SW influenced the displacement of oil and left smaller residual oil clusters in the porous space than the DW flood. This can be seen from the Lorenz plot (c) and cluster analysis (d) in Figure 5.6.

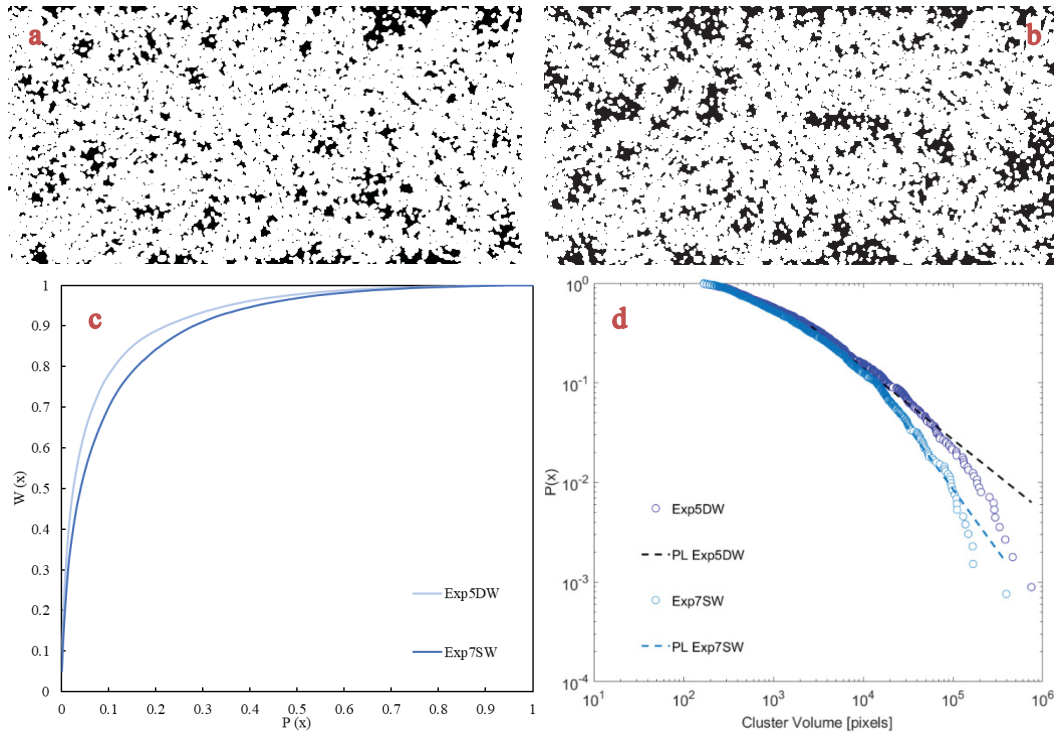


Figure 5.6 – a) Exp. 7 after SW, b) Exp. 5 after DW, c) Lorenz Plot, d) Cluster Analysis

Although the end state images of Exp. 12 and Exp. 13 (Figure 5.7) looked quite different from previous water flooding scenarios, they both were in the overall range of secondary RFs. The secondary recovery of Exp. 12 was slightly higher than of Exp. 13, but the normalized Euler number was lower. Both their water floods did not reach a water-wet state in the model.

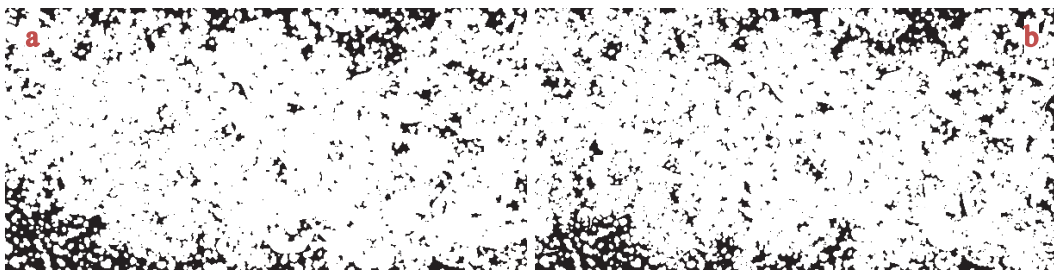


Figure 5.7 - left: Exp. 12 after SW flooding, right: Exp. 13 after SW flooding

The Lorenz plot and cluster analysis in Figure 5.8 suggest that Exp. 12 and Exp. 13 had very similar residual cluster sizes and oil volumes present in the porous medium.

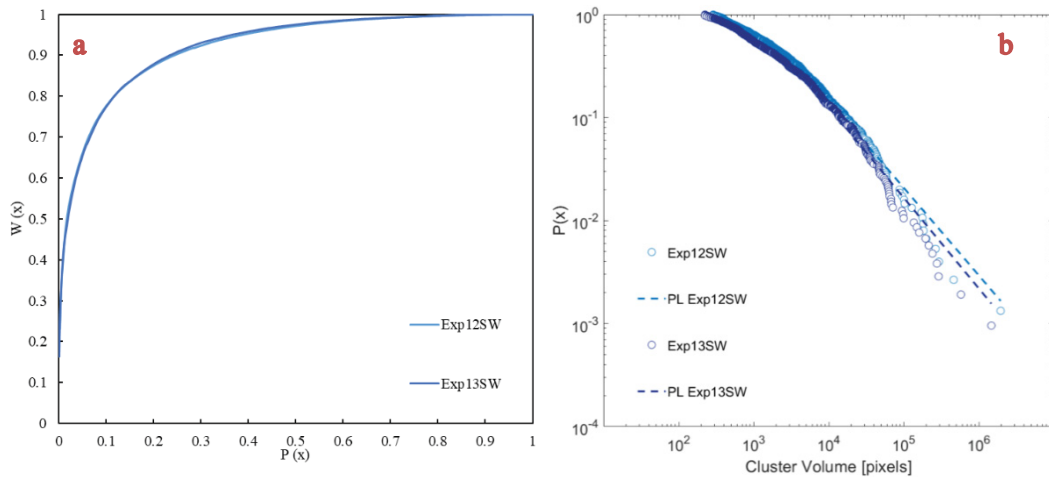


Figure 5.8 – Exp. 12 and 13 SW: a) Lorenz plot and b) Cluster Analysis

When comparing the cluster analysis from SW flooding results of Exp. 7 and Exp. 13 (Figure 5.9) it could be seen that Exp. 13 had overall bigger clusters with a larger probability of containing residual oil left in the model. The power law maximum likelihood function of Exp. 7 did not fit the resulting curve properly which could happen in some cases and depends on the curvature of the given data set.

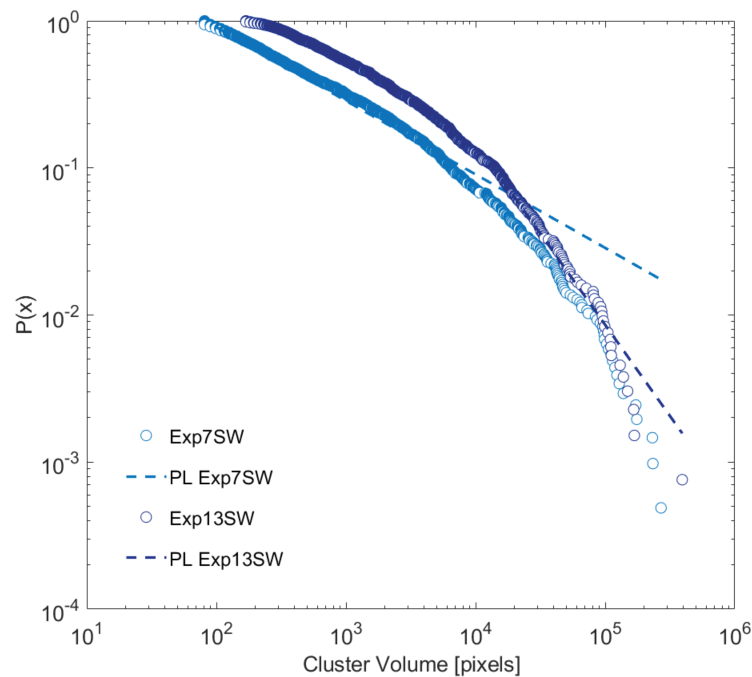


Figure 5.9 - SW flood Exp. 7 and Exp. 13 Cluster Analysis

The Lorenz plot (Figure 5.10) confirmed that the EOR potential of Exp. 7 was the smallest compared to all other water flooding experiments and has produced more oil during the SW flood than all other water flooding experiments (Table 5.1).

The biggest EOR potential showed Exp. 6 which had the big oil cluster left in one corner (Figure 5.3) and Exp. 11 (see chapter 5.3).

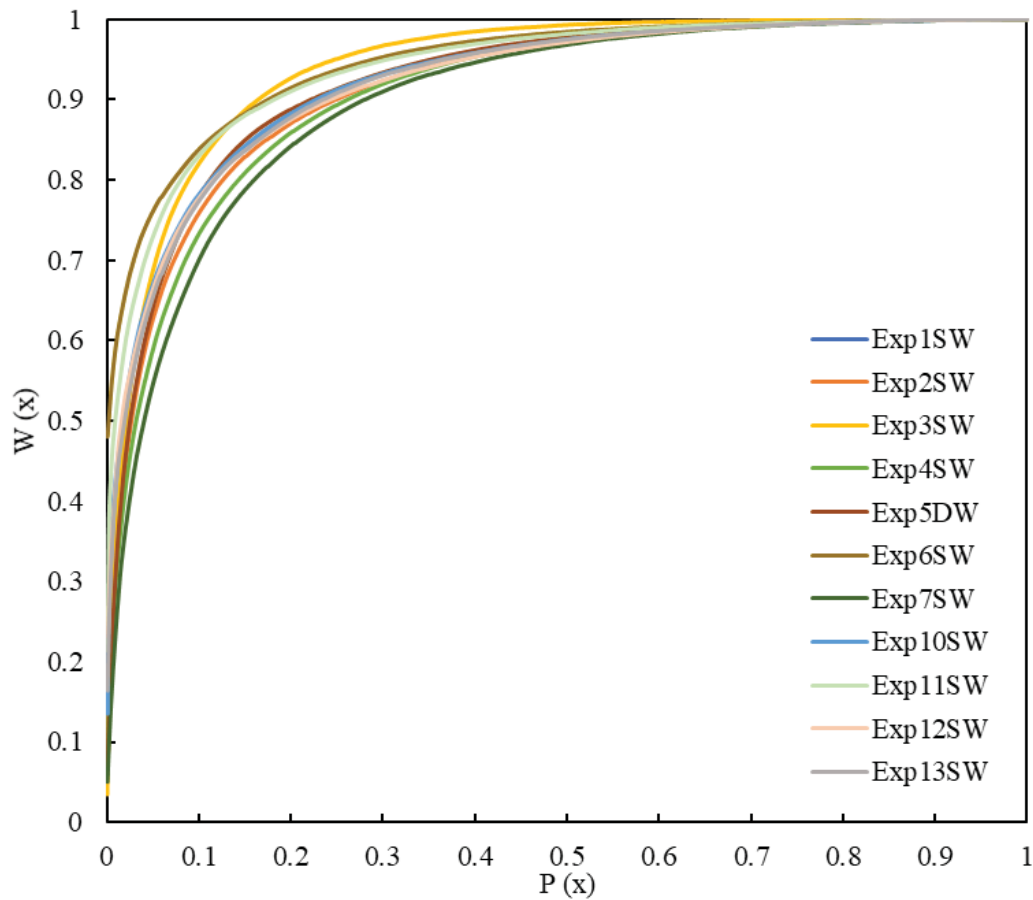


Figure 5.10 - Lorenz Plot of Water flooding

5.2 Alkaline Flooding

The concentration of 3000ppm was initially seen as the target alkaline concentration since it has been very promising in a study with a similar crude oil with a slightly higher TAN number. Therefore, the first couple of experiments focused on an alkali range from 200ppm to 3000ppm in SW. Furthermore, a comparison to DW with alkaline flooding as well as the application of reservoir temperature to experiments with an alkali concentration of 3000ppm were of interest.

The alkaline flooding scenarios lead to ultimate recovery factors between 65% and 90% (Table 5.1). Figure 5.11 gives a schematic overview of how the secondary recovery factors after water flooding changed to the ultimate recovery factors after alkaline flooding as well as the impact of change in total ionic strength (TIS).

When alkaline flooding was applied in combination with SW, the TIS became greater with respect to the alkaline content. In Exp. 7 and Exp. 11 where alkali salt dissolved in DW was injected after a SW flood, the TIS decreased during alkaline flooding. Those experiments both resulted in a positive tertiary recovery compared to other alkaline flooding experiments up to 3000ppm which did not achieve significant tertiary recovery. Although a reduction in TIS

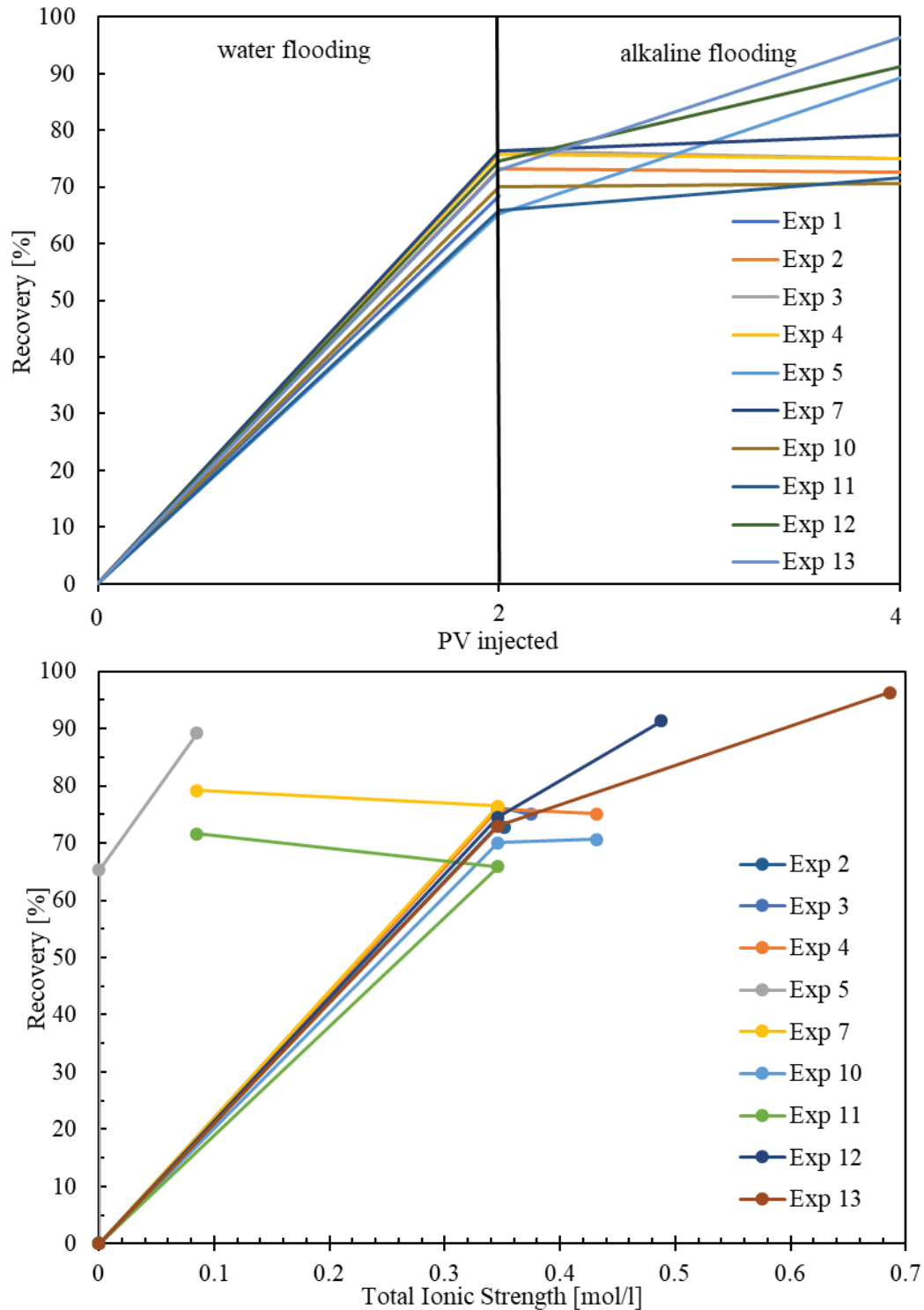


Figure 5.11 – Ultimate Recovery vs. PV injected and total ionic strength (TIS)

improved recovery (Exp. 7 and Exp. 11), further increasing the TIS by using a higher alkali concentration achieved a greater ultimate recovery (Exp. 12 and Exp. 13).

Exp. 5 (DW as water flood, followed by DW3000) achieved the highest tertiary recovery but not the highest ultimate recovery. Since that experiment could not be related to any realistic reservoir condition it was interesting to see if there would be a relationship between the ratio of alkali to TDS in the solution and the tertiary recovery.

Figure 5.12 shows tertiary recovery of SW and DW flooding experiments in relation to alkalinity of the regarding solutions. The dotted line suggests a possible trend which would state that from a certain alkalinity ratio the tertiary recovery would not significantly change. However, this would require further investigation at higher alkaline solutions as well as with different crude oils. The only experiment with 100% alkalinity was Exp. 5 (DW in water flooding and DW3000 during alkaline flooding).

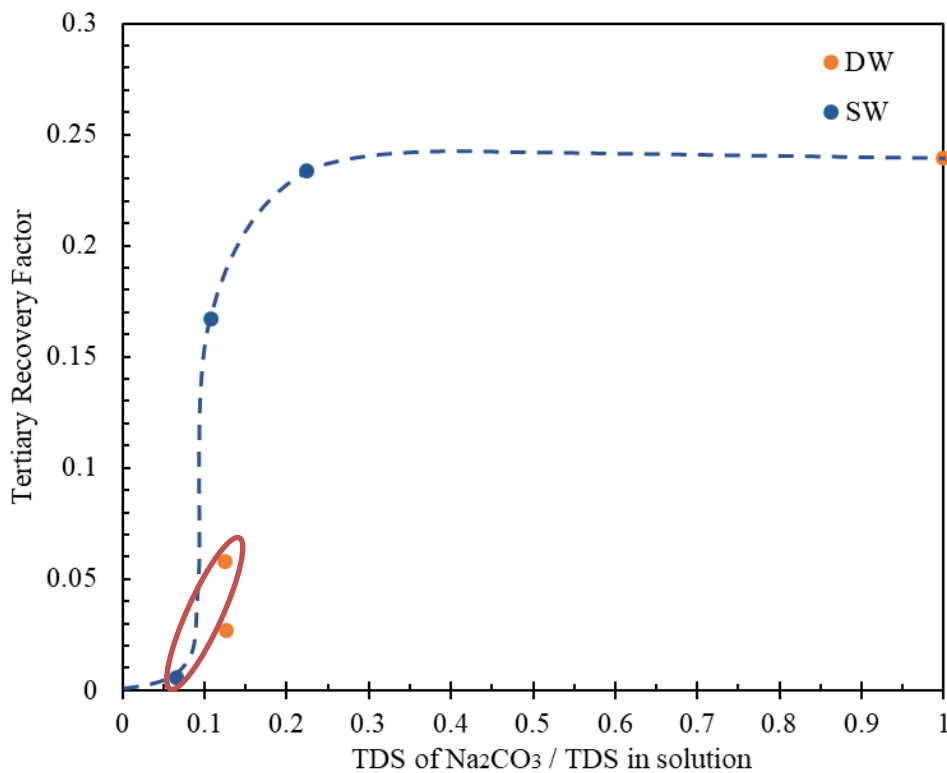


Figure 5.12 - Alkalinity effect on tertiary recovery.

The red oval marks the data points of Exp. 10 and Exp. 11 which were carried out at reservoir temperature conditions and resulted in higher tertiary recovery than their related experiments at ambient temperature conditions. The dashed line is a guide to the eye for alkalinity influence on tertiary recovery.

DW with alkali after SW as water flood (Exp. 7 and Exp. 11) resulted in a small but positive tertiary recovery while SW with an alkaline concentration up to 3000ppm did not show a significant change in recovery after water flooding with SW (upper plot in Figure 5.13).

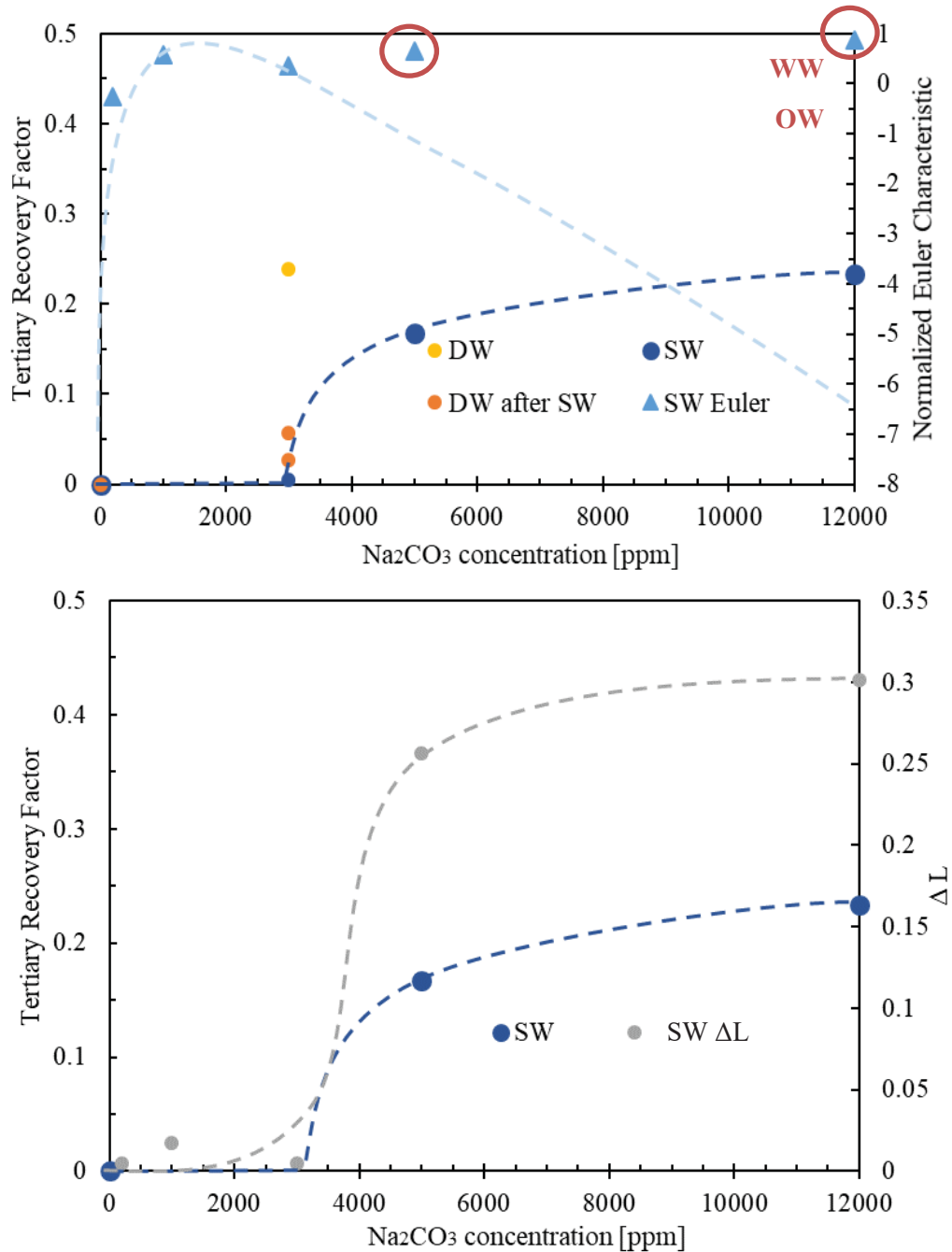


Figure 5.13 – Top: Concentration effect on tertiary recovery (circle markers) and normalized Euler characteristic (triangular markers).

The red circles mark two data points (from Exp. 12 and Exp. 13) in the water-wet (WW) region (positive normalized Euler characteristic) which were not in agreement with their actual wettability state which was oil-wet(OW) as indicated by the respective guide to the eye (light blue dashed line). Bottom: Concentration effect on ΔL which represents the region between the curves after water and alkaline flooding in the Lorenz plot.

The normalized Euler number results suggested a water-wet state from an alkali concentration of 1000ppm upwards (top plot in Figure 5.13). For Exp. 12 with 5000ppm and Exp. 13 with 12000ppm alkali concentration this water-wet state was not truly reached because a very thin oil film was completely covering the grains which only became visible at a magnification of 20x (Figure 5.32 in chapter 5.4). For the normalized Euler characteristic plotted in Figure 5.13, the guide to the eye was drawn according to the truly observed wettability state in the respective experiments.

The trend of increasing tertiary recovery with alkaline concentration suggested that some of the residual oil in individual clusters connected and were mobilized during this wettability transition (water-wet after water flooding to oil-wet after alkaline flooding).

Detailed evaluation and comparison of individual alkaline flooding results

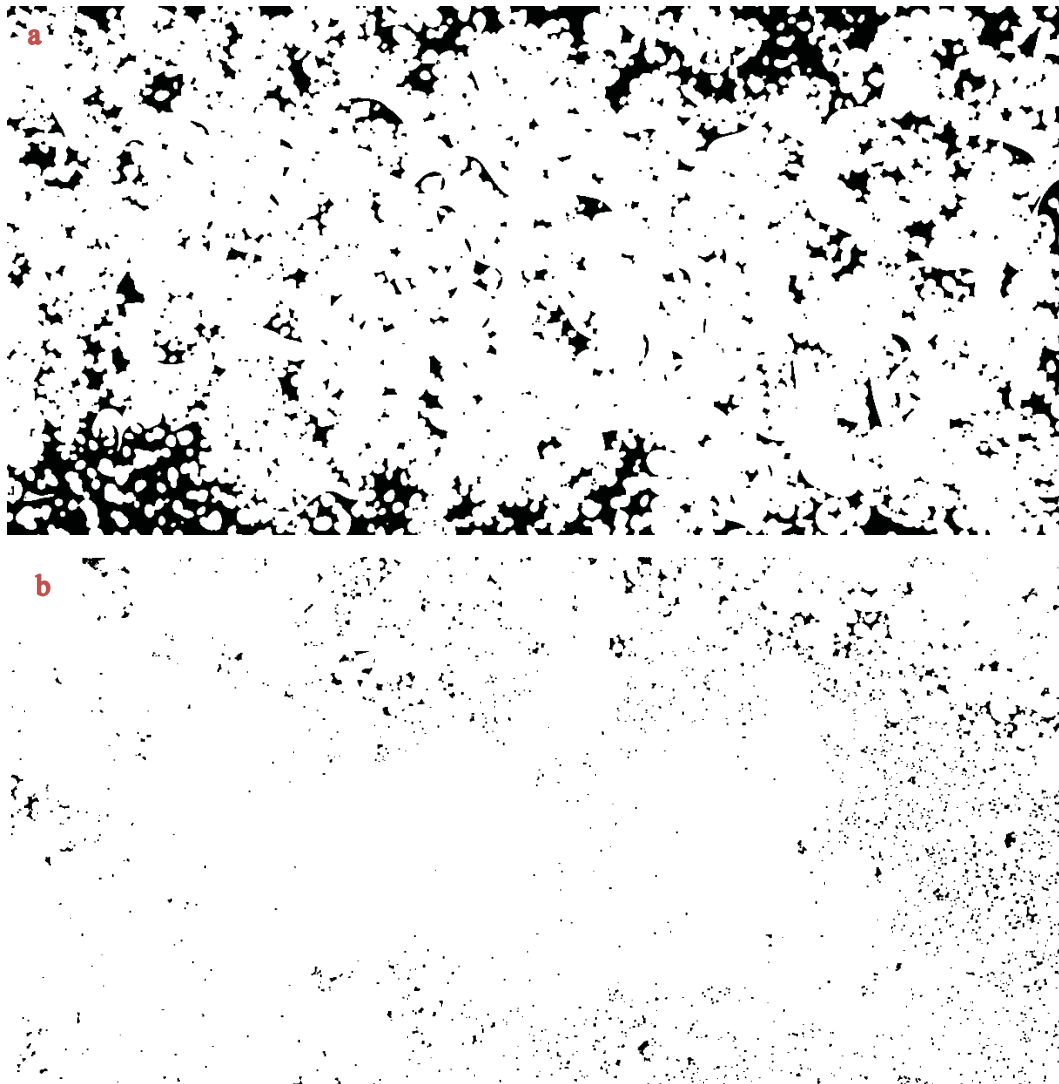


Figure 5.14 - Exp. 13 a) after water flooding, b) after alkaline flooding

The highest ultimate recovery was achieved in Exp. 13 carried out at ambient temperature conditions with SW as water flood. As can be seen in Figure 5.14 (a), after water flooding many bigger oil clusters remained trapped. The alkaline flood of SW12000 contained the highest alkali concentration used in the frame of this work. In Figure 5.14 (b) are some small residual oil clusters visible, but those did not enclose whole grains in this processed picture. Mostly there were single droplets of oil left in the processed image which resulted in a positive normalized Euler number as mentioned before. This is where the processing of the pictures did not represent the real wetting state sufficiently. The thin oil film which actually covered the grain surface disappeared during image processing because it was not visible next to the thick

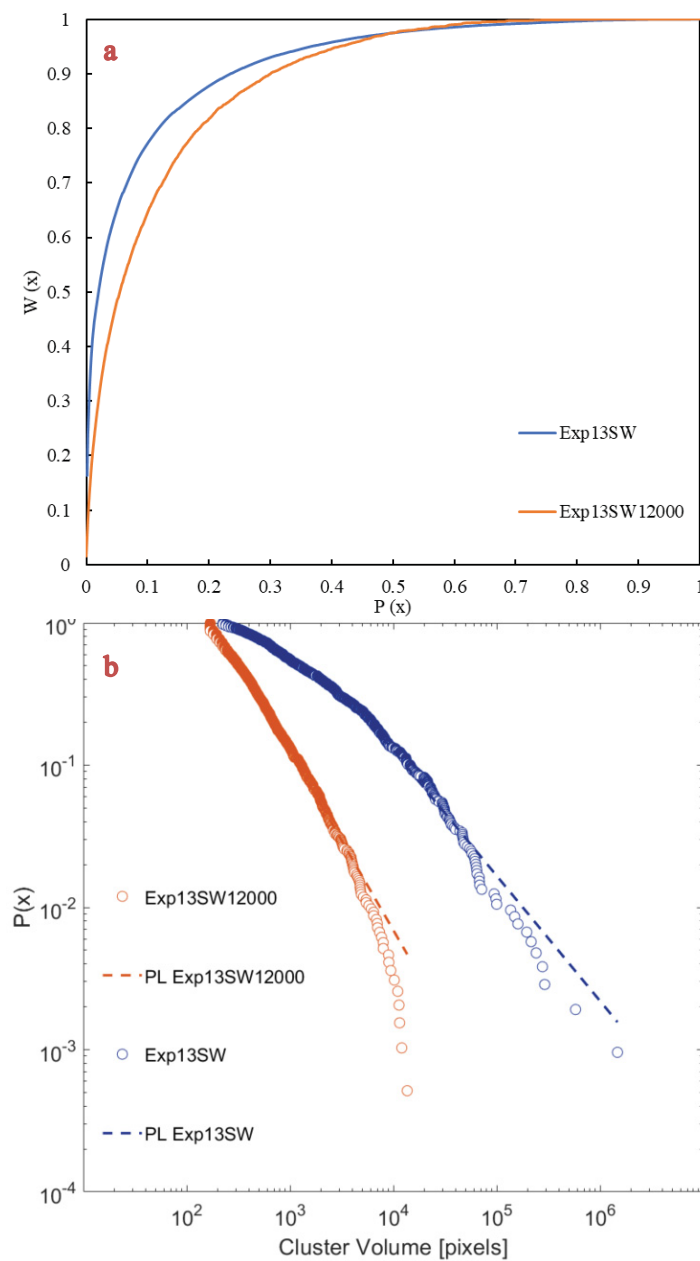


Figure 5.15 – Exp. 13 a) Lorenz Plot, b) Cluster Analysis

grain surfaces at the regular magnification of 2.5x which was used for image acquisition of the entire micromodel (chapter 4.2).

The Lorenz Plot of Exp. 13 (Figure 5.15, a) shows that the alkaline flooding did split up the big clusters and overall lead to a more equal distribution between cluster volume and the probability of residual oil inside. The cluster analysis (Figure 5.15, b) suggests that the cluster volume was reduced drastically. For the real case of Exp.13 (oil-wet system), it would be expected to result in showing one big residual oil cluster containing a very small amount of oil.

The second highest tertiary recovery was achieved by Exp. 5 which had DW as a water flood (Figure 5.16, a) and DW3000 as alkaline flooding (Figure 5.16, b). Figure 5.17 shows the volume cluster analysis for Exp. 5. The Lorenz plot shows a huge gap between the DW and DW3000 curves which confirms the high EOR potential after waterflooding and was very well utilized by the applied alkaline flooding.

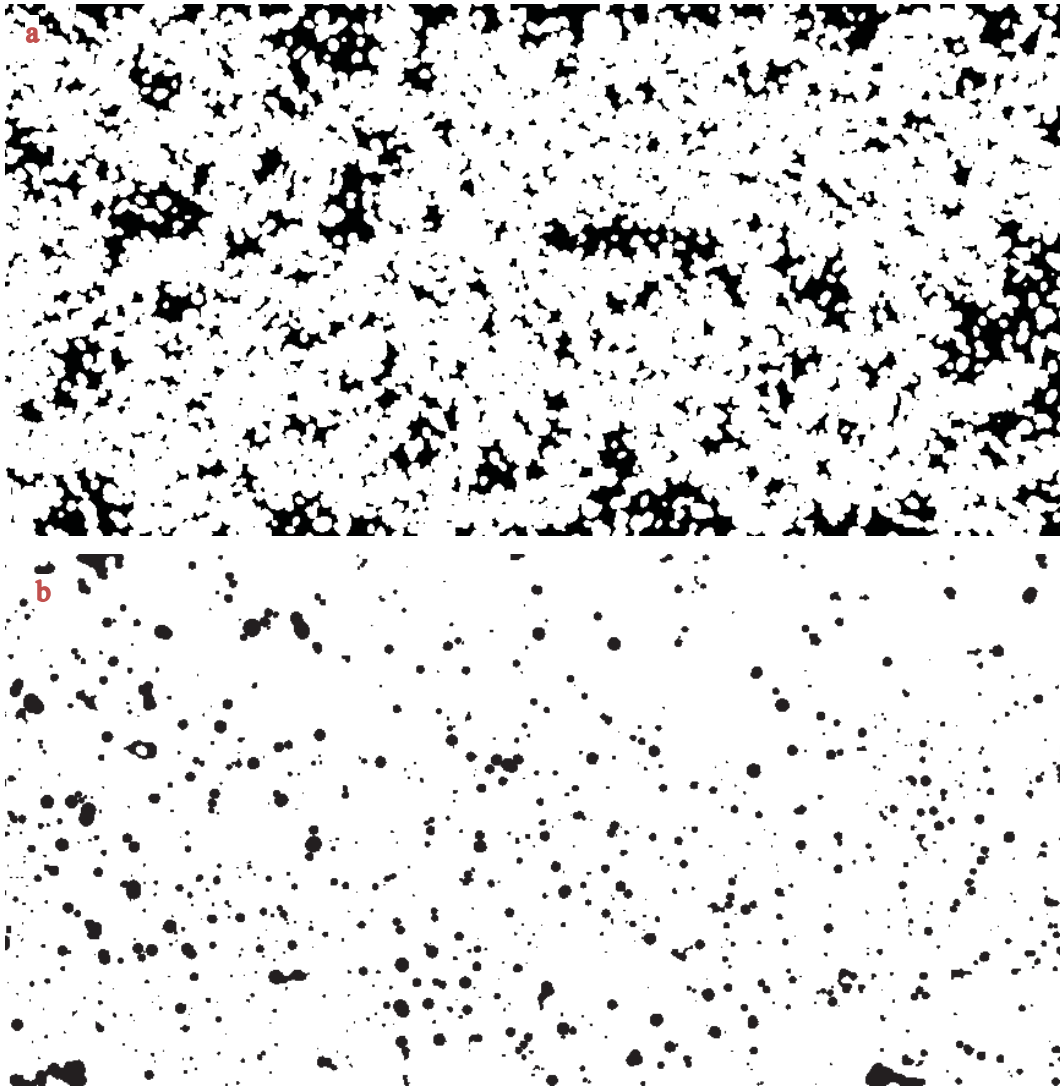


Figure 5.16 - Exp. 5 a) after DW flooding, b) after DW and DW3000 flooding

This was the only experiment which truly reached a completely water-wet state. It would have been expected to achieve the highest oil recovery, but as seen from Exp. 13, an oil-wet system can sometimes be more favourable for oil recovery. In the oil-wet case, residual oil clusters connected and formed new flow paths and the finally residual oil film sticking to the grains was of very small volume compared to the droplets which were stuck (oil entrapment) in the pore throats during Exp. 5 (Figure 5.16, b).

From the cluster analysis (Figure 5.17, b) can be seen that the number of big clusters was significantly reduced, and the greatest amount of oil volume remained in the medium big to

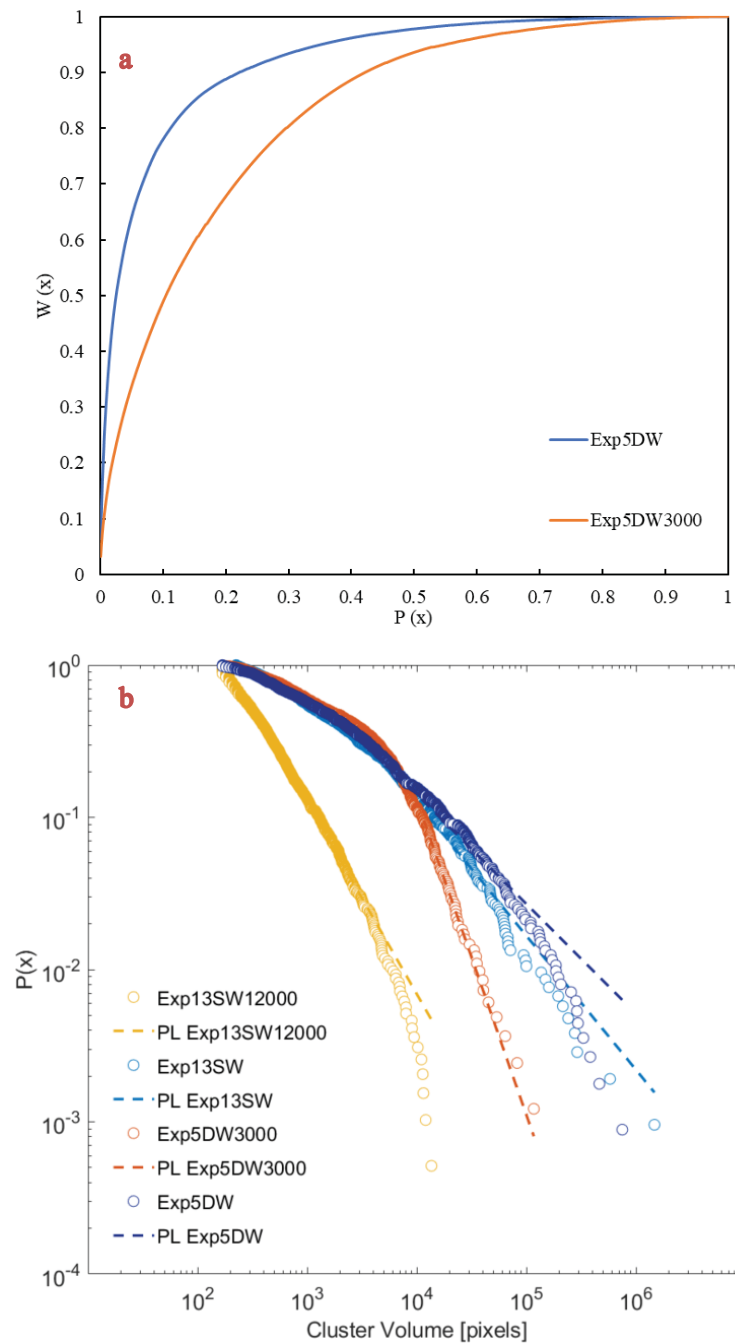


Figure 5.17 - Exp. 5: a) Lorenz Plot, b) Cluster Analysis compared to Exp. 13

small droplets. This corresponds reasonably to the images above (Figure 5.16). Further, it was clearly visible that Exp. 13 with SW12000 was much more effective in reducing cluster volumes during alkaline flooding than DW3000.

The second highest ultimate recovery was achieved in Exp. 12. The inlet channels which lead to the lower left corner of the micromodel were possibly blocked during water flooding as they cleaned out during alkaline flooding (compare a and b in Figure 5.18). There is a chance that additional oil entered the micromodel during alkaline flooding.

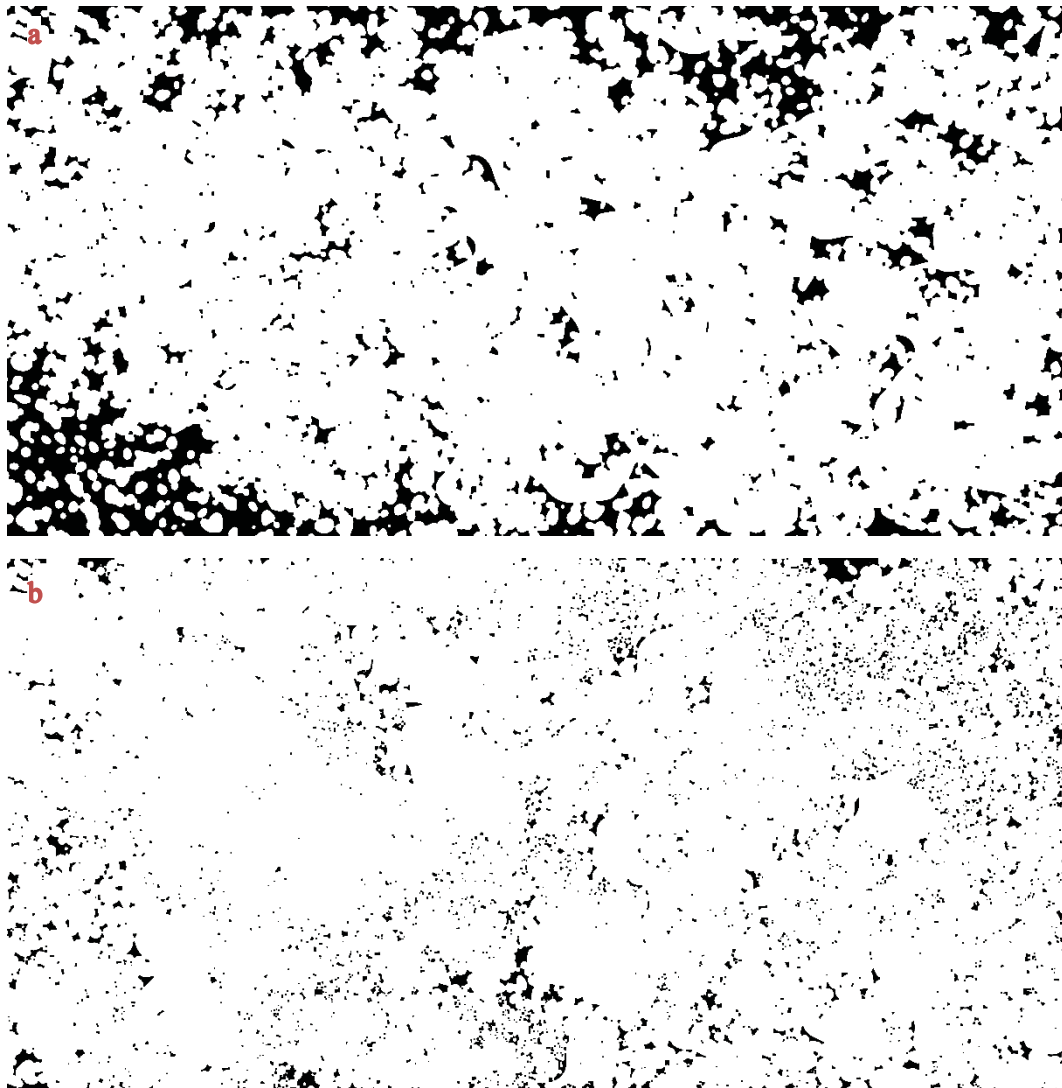


Figure 5.18 - Exp. 12: a) after water, b) after alkaline flooding

The Lorenz plot of Exp. 12 (Figure 5.19) is similar to the one of Exp. 13 (Figure 5.15) and shows that the alkaline solution with 5000ppm achieved similar results as 12000ppm despite the huge difference in concentration.

The lower plot in Figure 5.19 compares the cluster analysis of Exp. 12 and Exp. 13. Although the Lorenz plots look almost identically, the cluster analysis shows the difference which led to a slightly lower ultimate recovery in Exp. 12. There were some bigger residual clusters present after alkaline flooding, compared to Exp. 13.

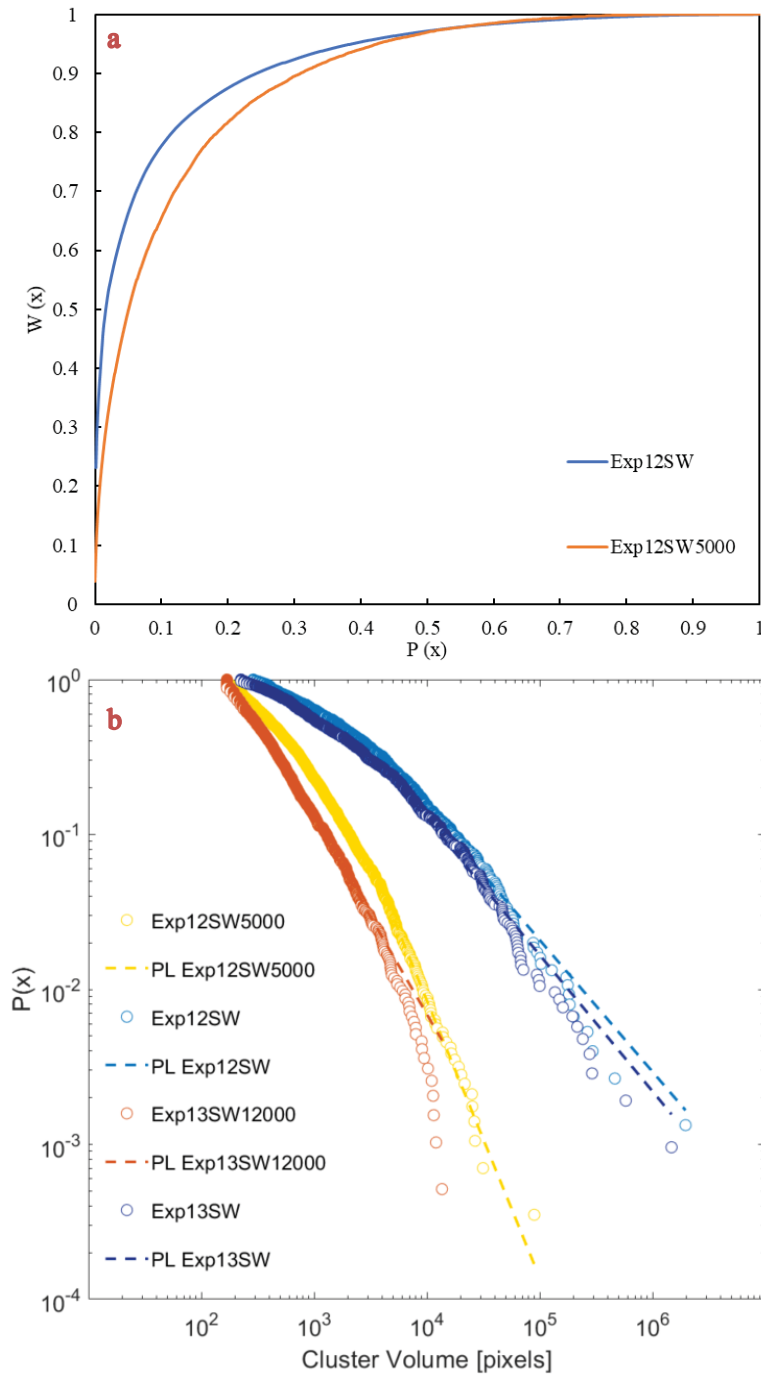


Figure 5.19 – a) Lorenz Plot Exp. 12, b) Cluster Analysis Exp. 12 and Exp. 13

Figure 5.20 (Exp. 7.) shows the WBT of the SW front during water flooding and the final state after water flooding with SW. In this experiment, the porous medium already became water-wet during the waterflood. It was visible how the big oil clusters were broken up during alkaline

flooding and at the same time oil remained trapped in clusters around grains and as droplets in pore throats.

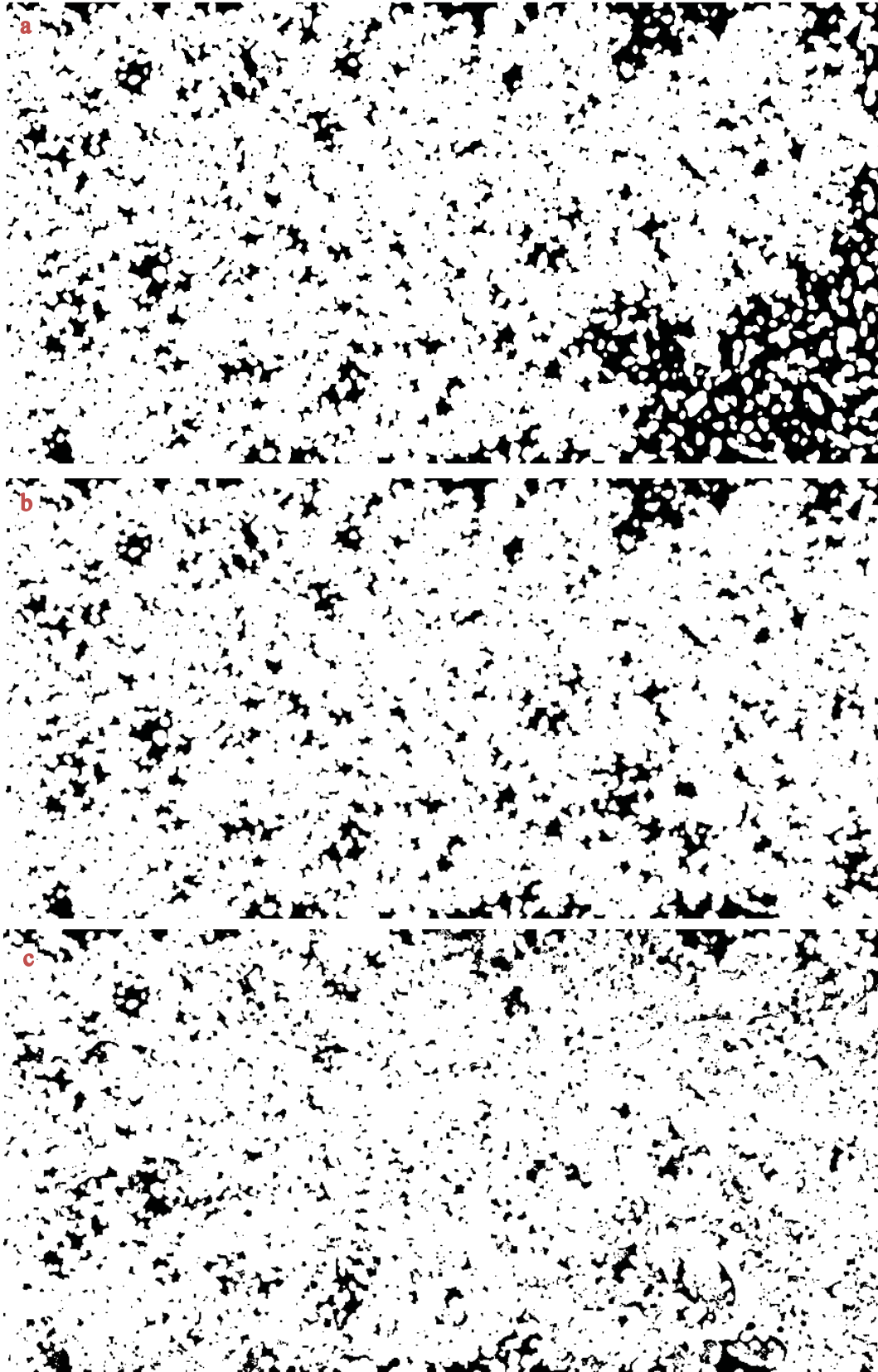


Figure 5.20 – Exp 7: a) Water Break Through (WBT) b) after SW c) after SW and DW3000

The normalized Euler number after alkaline flooding was slightly negative which indicates an oil-wet system. The areas where emulsion had formed might have caused some small pixel holes in oil clusters during image processing and caused this negative normalized Euler number.

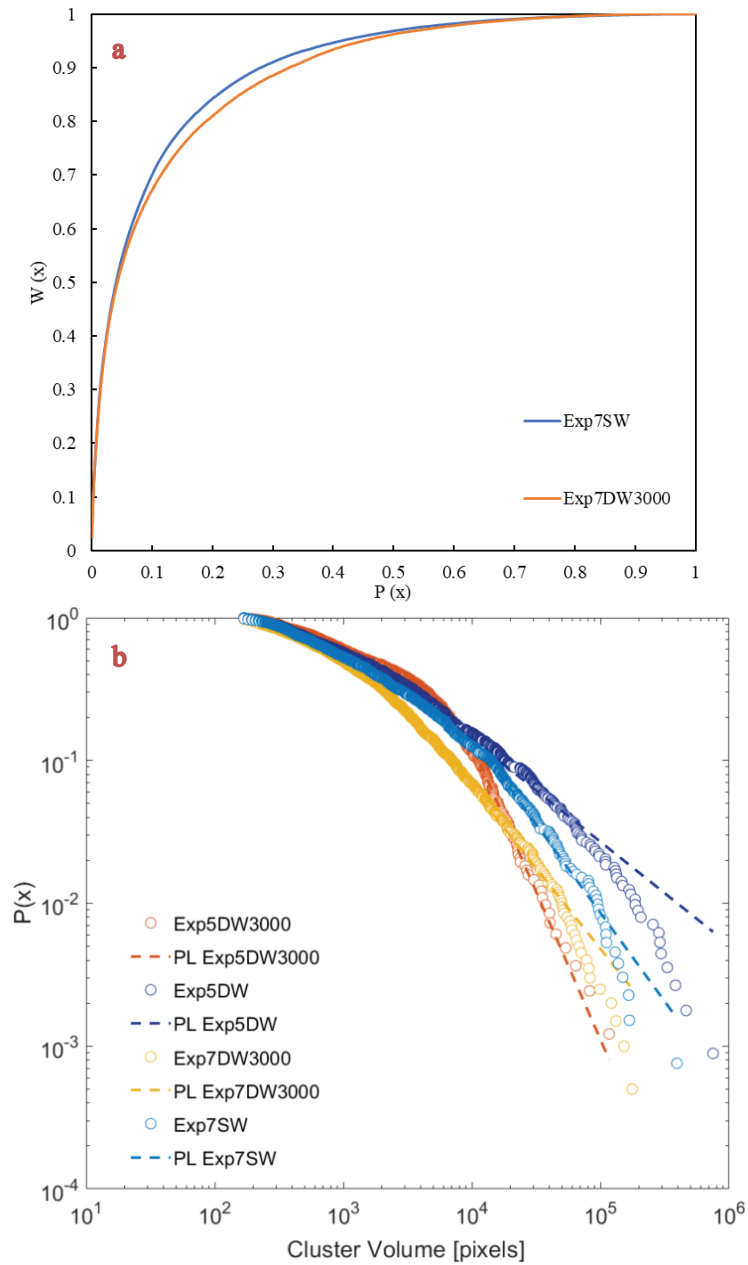


Figure 5.21 – Exp. 7: a) Lorenz plot, b) Cluster Analysis compared to Exp. 5

Visually, wettability did not change much during alkaline flooding in Exp. 7, therefore some bigger clusters of oil did break up due to viscous forces but could not entirely be mobilized. The cluster analysis in Figure 5.21 helps visualizing how small the change in this scenario was compared to Exp. 5.

The highest tertiary recovery following a SW flood reached Exp. 6 which had the largest EOR potential left due to its heterogeneous displacement pattern from water flooding (image a in Figure 5.22).

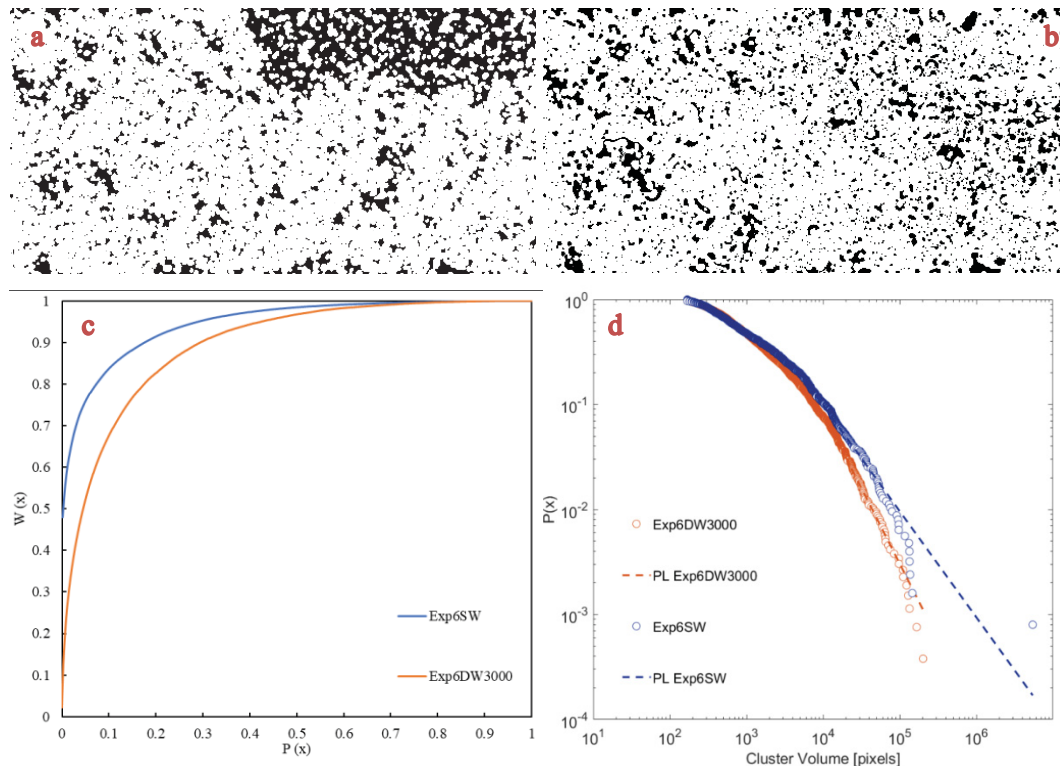


Figure 5.22 - Exp. 6: a) after SW, b) after SW3000, c) Lorenz plot, d) Cluster Analysis

The Lorenz plot (image c in Figure 5.22) shows a great ΔL between the SW and SW3000 flood which is mostly caused by this one big residual cluster of oil which can also be seen in the cluster analysis as the one single dot at the lower end of the Exp6SW curve.

Exp. 2, Exp. 3 and Exp. 4 resulted in similar ultimate recovery factors and a small negative tertiary recovery (Table 5.1) which showed that alkaline flooding with SW and alkaline concentrations up to 3000ppm were not very effective after water flooding with the given SW. Figure 5.23 shows the resulting images for Exp. 2, Exp. 3 and Exp. 4.

The normalized Euler number was positive after both, water and alkaline flooding of Exp. 3 and Exp. 4, which therefore remained in their water-wet state throughout alkaline flooding.

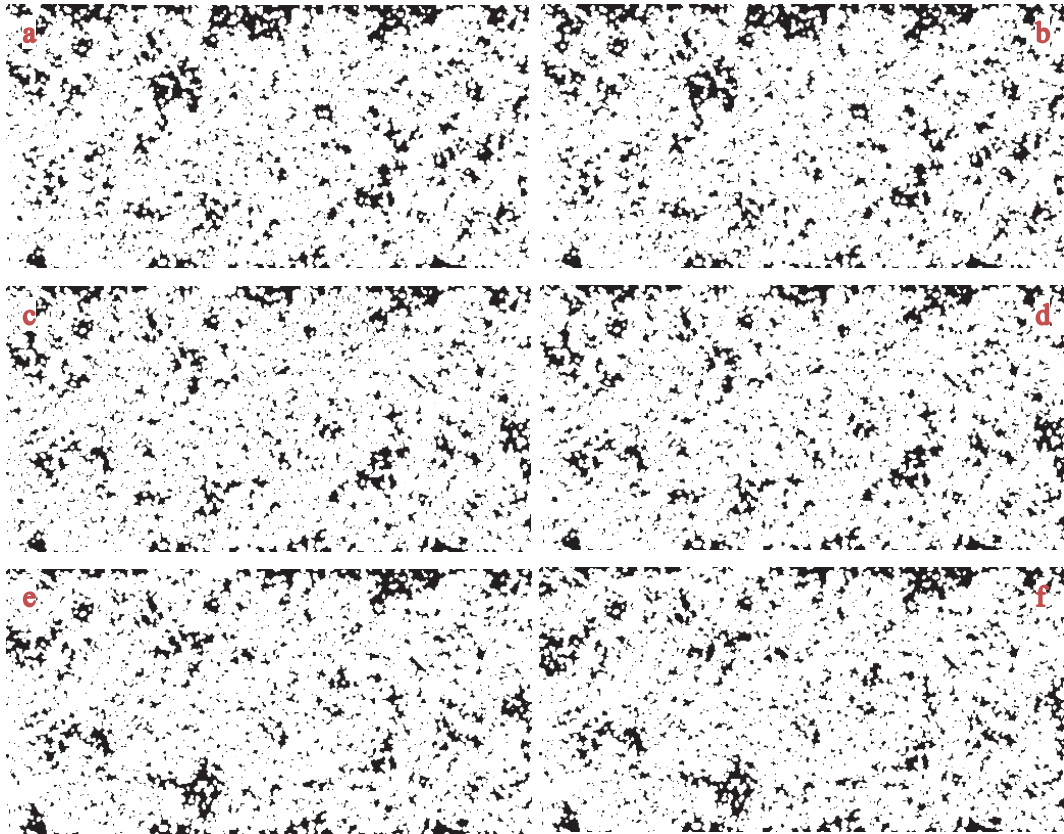


Figure 5.23 - Exp. 2: a) after SW, b) after SW200, Exp. 3: c) after SW, d) after SW1000, Exp. 4: e) after SW, f) after SW3000

Figure 5.24 shows the Lorenz plots of Exp. 2, Exp. 3 and Exp. 4 and directly compares alkaline flooding of 200ppm, 1000ppm and 3000ppm in SW after water flooding with SW. In Exp. 2 and Exp. 4 the changes from water to alkaline flooding were insignificantly small which can be seen in the images (Figure 5.24) and their resulting recovery factors (Table 5.1).

Exp. 3 with SW1000 as alkaline flooding after SW showed a small change in the Lorenz plot and cluster analysis which occurred due to a higher EOR potential of the SW flood in Exp. 3 compared to the other water floods.

Finally, neither SW with 200ppm, 1000ppm nor SW with 3000ppm were considered to be more effective than water flooding with SW itself that already reached a water-wet state as indicated by their normalized Euler number results and equally high recovery factors (Table 5.1).

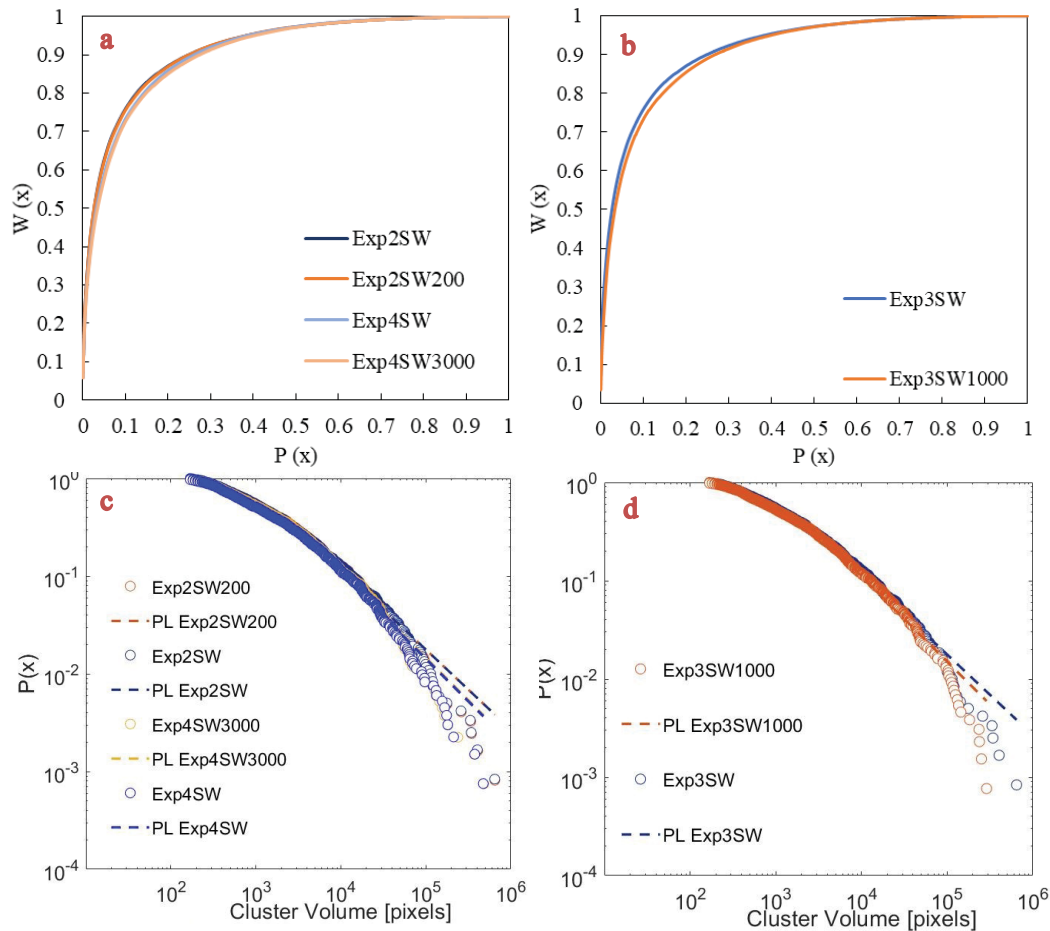


Figure 5.24 - Lorenz Plot and Cluster Analysis

a) & c) Exp. 2 (SW followed by SW200) and Exp. 4 (SW followed by SW3000), b) & d) Exp. 3 (SW followed by SW1000).

Figure 5.25 compares the cluster analysis of the experiments with alkali concentrations from 3000ppm to 12000ppm after SW flooding. The cluster sizes and volumes of the individual SW flooding experiments were similar to each other and to the alkaline flooding experiments up to 3000ppm as shown before. With increasing alkalinity, the cluster sizes and volumes were further reduced, hence the curves in Figure 5.25 shifted to the left.

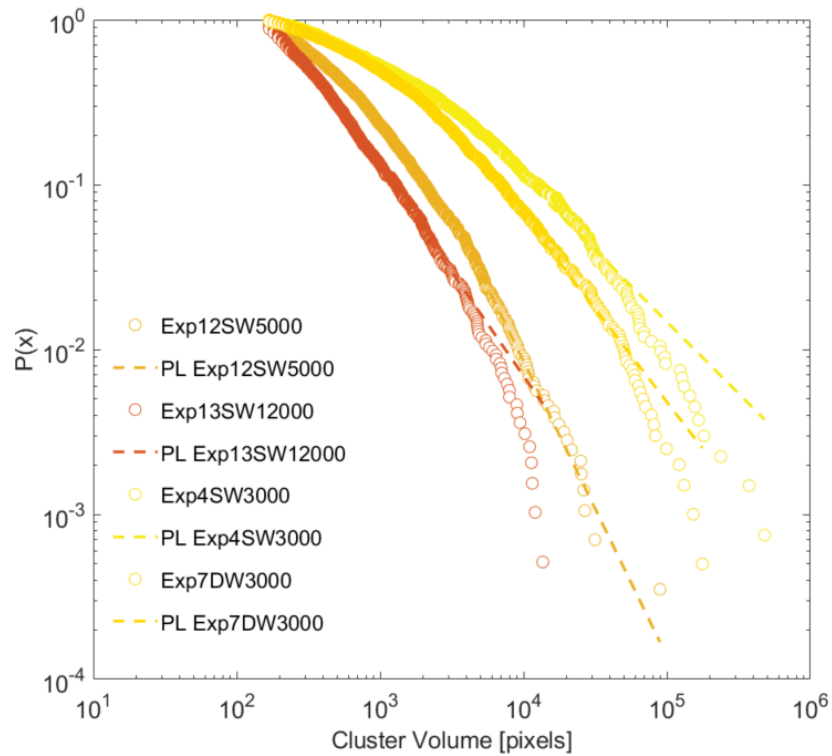


Figure 5.25 - Cluster Analysis: alkaline flooding comparison after SW flooding (3000ppm to 12000ppm)

5.3 Flooding Experiments at Reservoir Temperature

Regarding the experiments at reservoir temperature (60°C) Exp. 8 and Exp. 9 could be seen as first trial runs which had to be repeated due to issues with image acquisition as well as analysis. Therefore, their results are not presented in detail.

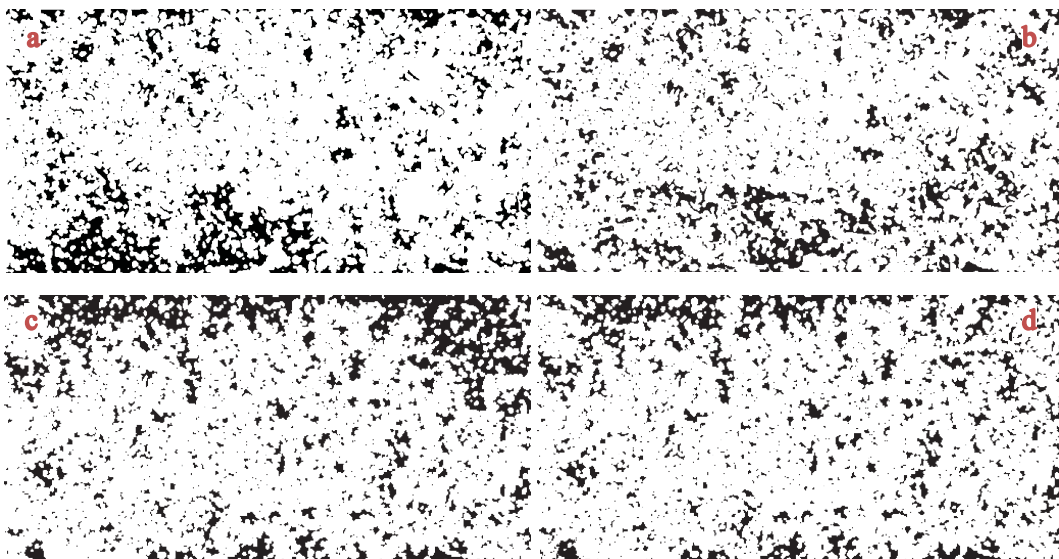
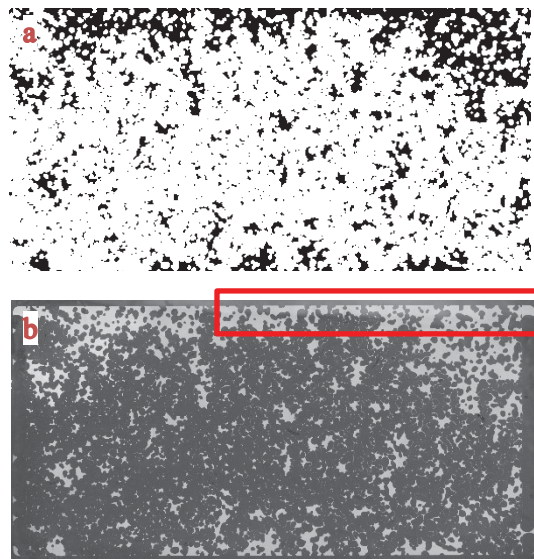


Figure 5.26 - Exp. 10 at 60°C: a) after SW, b) after SW3000, Exp. 11 at 60°C: c) after SW, d) after DW3000

The WBT in experiments at reservoir temperature conditions occurred after almost 50 minutes compared to 55 minutes on average for ambient temperature conditions. Considering the temperature difference of 37°C, WBT was expected to occur much earlier at reservoir temperature because of a lower viscosity of the fluids.

The experiments at reservoir temperature conditions were represented by Exp. 10 and Exp. 11. Both performed water flooding with SW and were followed by SW or DW, each containing 3000ppm alkali, as shown in Figure 5.26. The images of the two water flooding experiments looked completely different compared to previous results. This could have various reasons. The first reason would be that Exp. 11 was performed on a new micromodel. Secondly, in all experiments at reservoir temperature (including the experience with Exp. 8 and Exp. 9) an issue of evenly distributing the temperature over the whole model repeatedly arised since the metal block did not exactly fill out the core holder opening above the micromodel. This led to temperature loss at one side of the model. By applying heat conductive paste over the entire surface of the porous space in the model, this loss was minimized in terms of temperature but might still have affected fluid flow.



*Figure 5.27 - Exp. 11 water flooding at reservoir temperature conditions
a) binary image, b) original image with fluorescent light; red box marks area which shows light reflections, hence was not completely covered by the metal block.*

Figure 5.27 shows both, the binary and the original picture at the end of water flooding in Exp. 11 and a red square marks the area which was not completely covered by the metal block. In this case, the upper part of the model did contain significantly more residual oil than the lower part.

The metal block was removed for cleaning purposes between the experiments, which is why it was placed differently during Exp. 10 which contained more residual oil in the lower part of the model after water flooding (image a in Figure 5.26).

The normalized Euler number increased during alkaline flooding at reservoir temperature, the end state, however, was still oil-wet (Table 5.1). The cluster analysis plot (b and d in Figure 5.28) shows how some of the big clusters were reduced in size in both experiments. The difference between water and alkaline flooding curves in the Lorenz plots (a and c in Figure 5.28) was bigger than for their related experiments at ambient temperature conditions. Furthermore, the tertiary recovery was higher for the experiments at reservoir temperature conditions (Table 5.1). This proves that while the secondary recovery was lower, alkaline flooding itself was more successful at reservoir temperature conditions.

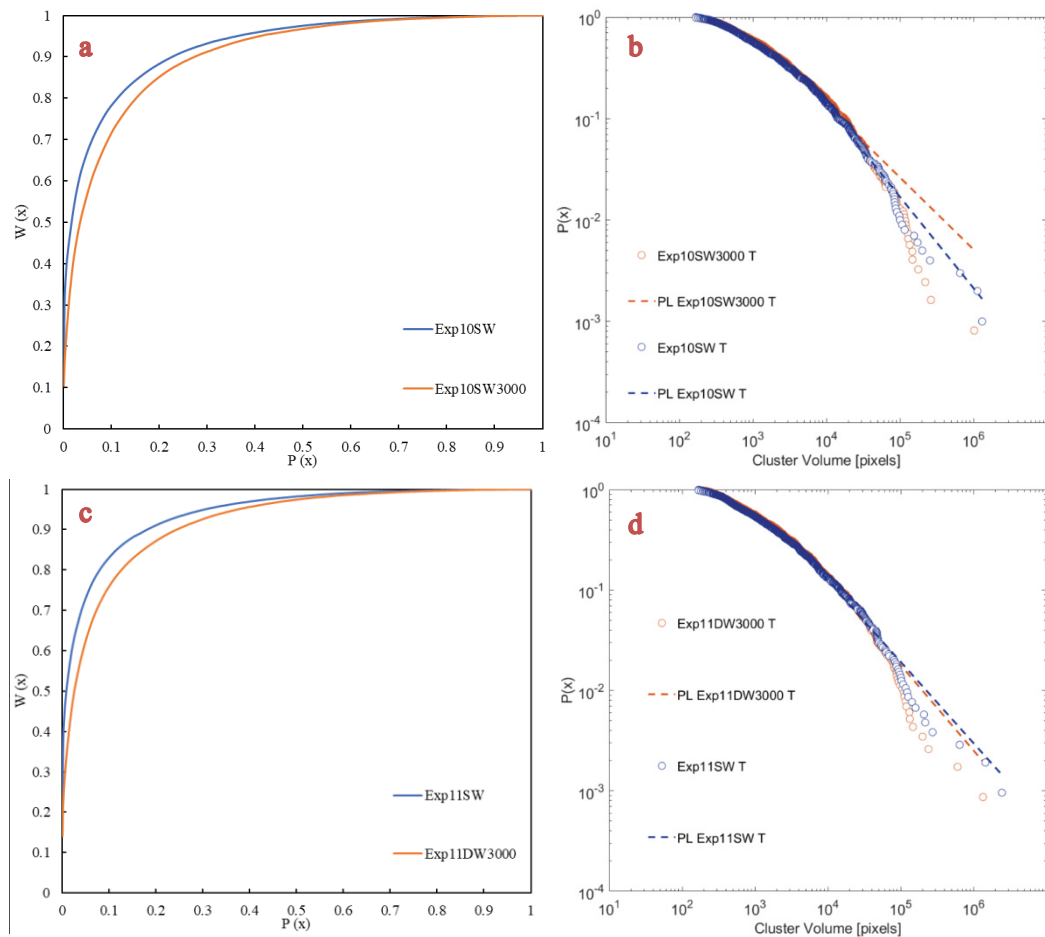


Figure 5.28 - Lorenz Plot and Cluster Analysis Exp. 10: a) & b), Exp. 11: c) & d)

5.4 Phase Behaviour

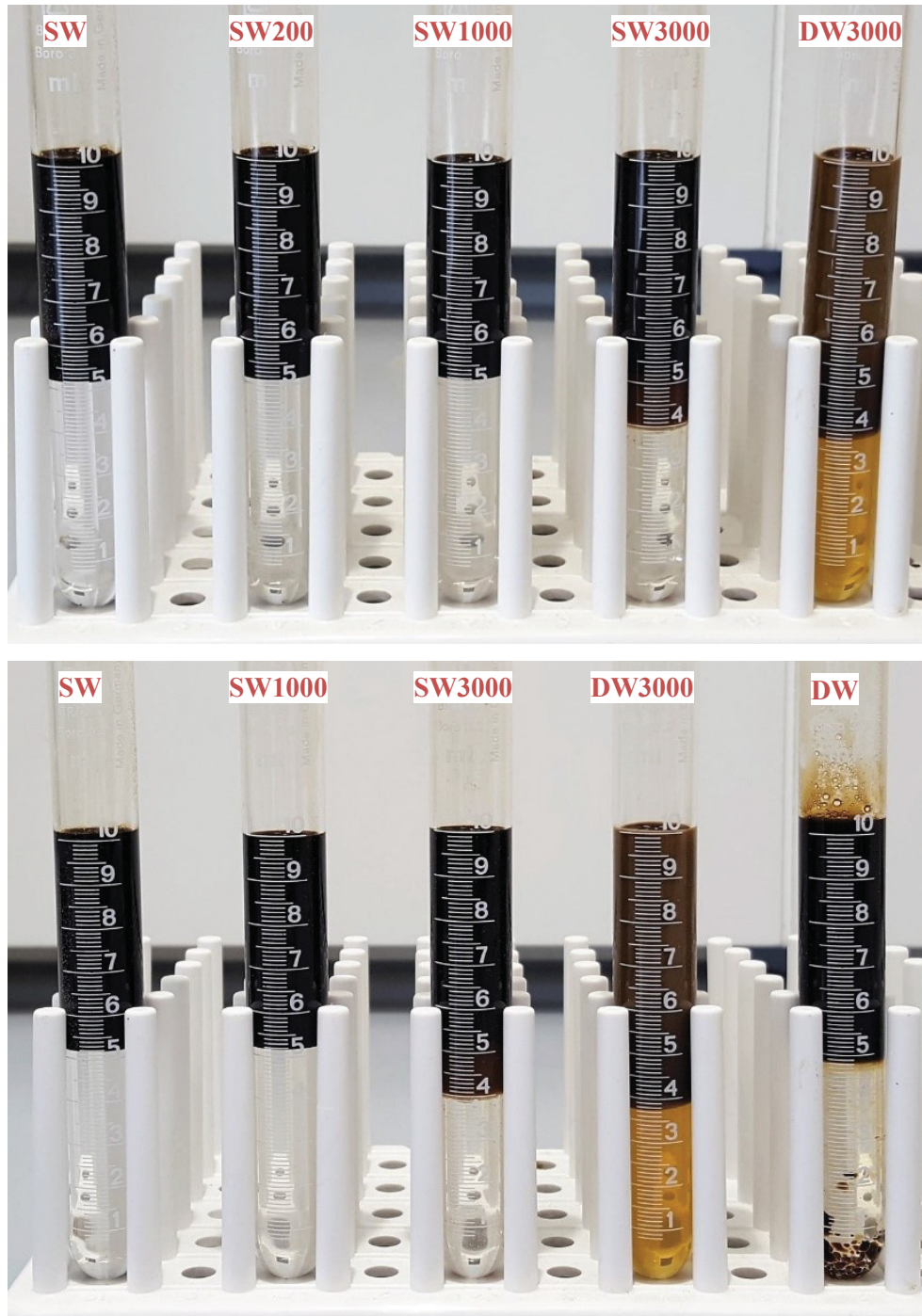


Figure 5.29 - PB at ambient temperature (0ppm to 3000ppm)

The phase behaviours tests that mixed oil with SW, SW200 and SW1000 remained coexisting as separate phases which correlates with the results in the microfluidic experiments of the respective concentrations where no mixing could be seen during laminar flow conditions.

SW with 3000ppm showed W/O emulsion and oil swelling (Figure 5.29) while the water phase on the bottom remained completely clear. SW3000 in Figure 5.29 showed an emulsion phase in lighter colour between the marks of 4ml and 5 ml.

In the test tube with DW and oil, the oil droplets stuck to the glass wall in the water phase. In DW3000, oil swelling occurred as well as O/W and W/O emulsions as can be seen from the different coloured phases in Figure 5.29. This alkali solution was applied the only microfluidic experiment where the porous medium became completely water-wet after flooding (Exp. 5, DW-DW3000). All residual oil and emulsions were trapped as droplets of different sizes in pore throats as shown in Figure 5.30.

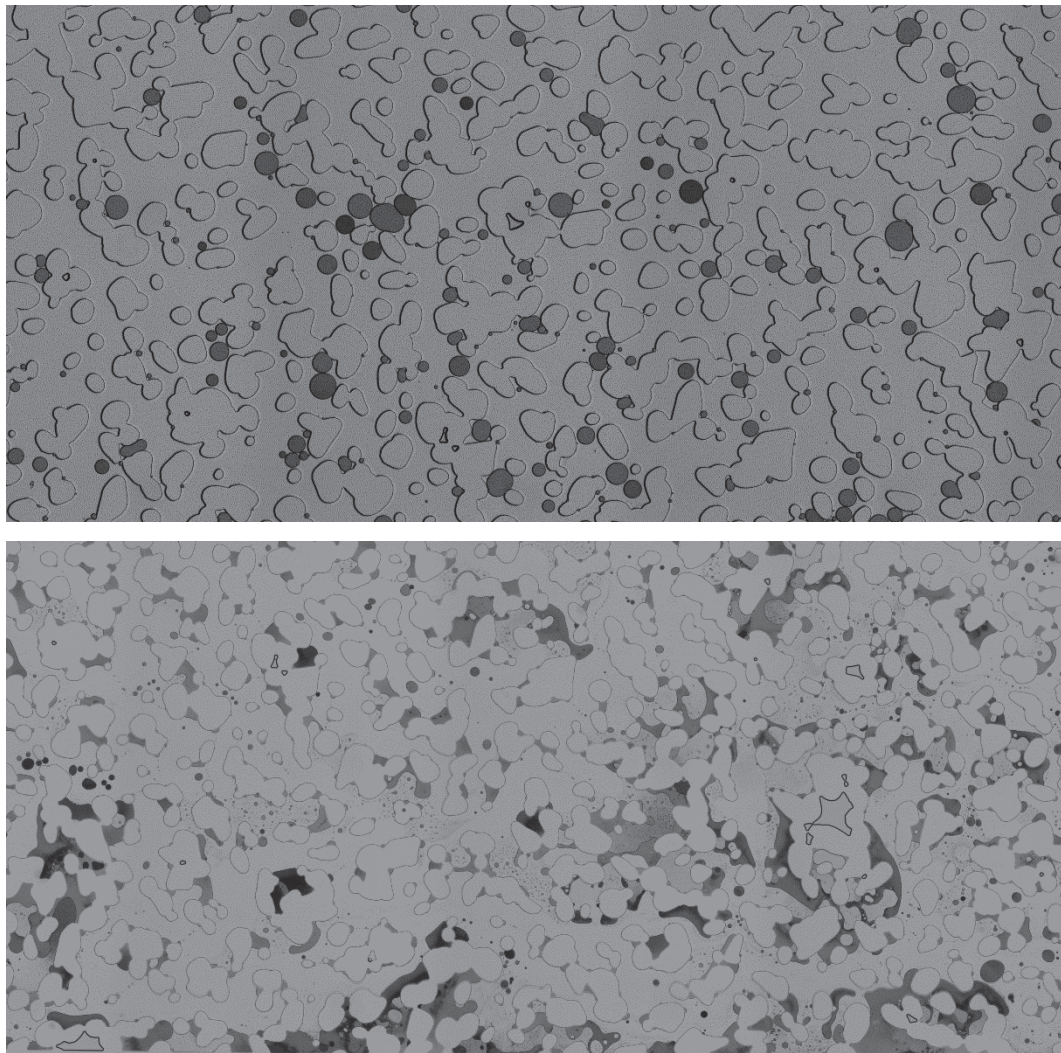


Figure 5.30 - Emulsion formation during Exp. 5 (top) and during Exp. 7 (bottom).

Emulsion phases are darker coloured residual oil droplets and clusters in above pictures.

Exp. 7 (SW-DW3000) also showed both, O/W and W/O emulsion formation during alkaline flooding, similar to the test tube of DW3000. The porous medium was partly water-wet and partly wetted by oil or emulsion. The black coloured oleic phase in Figure 5.30 show an instable microemulsion in the micromodel.

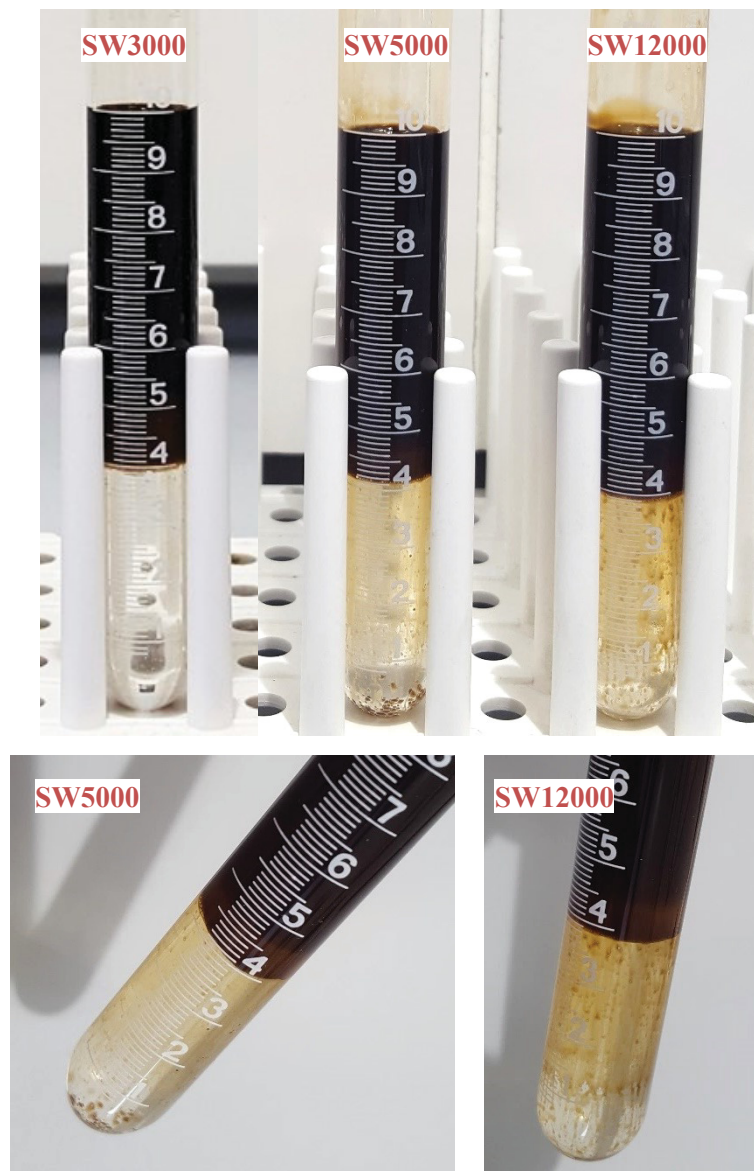


Figure 5.31 – PB at ambient temperature (3000ppm to 12000ppm)

Note that for SW5000 and SW12000 emulsion bubbles were sticking to the glass.

The SW3000 after SW experiment (Exp. 4) did not form emulsions at ambient temperature. The comparison between 3000ppm, 5000ppm and 12000ppm test tubes at ambient temperature (Figure 5.31) showed the impact of water alkalinity and salinity for this crude oil. While the water phase in 3000ppm was completely clear, it had many oil and emulsion bubbles sticking at the bottom and sides of the glass for 5000ppm and 12000ppm. Additionally, there was an emulsion phase visible between the 4ml and 4.5ml mark. Both had O/W and W/O emulsions present and oil swelling in the same range as the 3000ppm phase behaviour test.

The small bubbles indicate that these tests did not (yet) form microemulsions which would occur as a separate phase. However, those oil bubbles were also visible under dynamic laminar flow conditions in Exp. 12 and Exp. 13 (Figure 5.32).

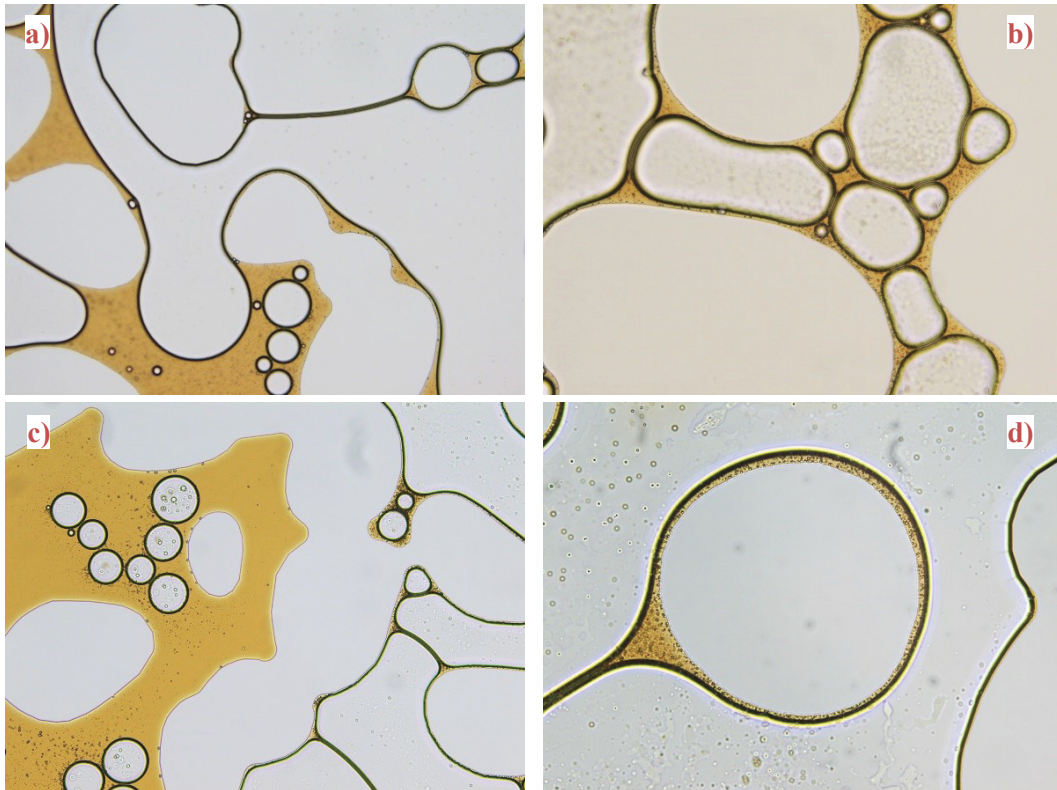


Figure 5.32 - Emulsion formation (Magnification 10x and 20x): a) & b) Exp. 12, c) & d) Exp. 13

In both experiments, the porous medium was completely wetted by the oil/emulsion phase. Although they both had incredibly high ultimate recovery factors, on the microscale it was visible that these high salinity floods did not manage to completely bind and transport the oil phase. These experiments should have resulted in the greatest negative normalized Euler number of all flooding experiments since all grains were covered in a very thin oil/emulsion film.

There are both emulsions (O/W and W/O) clearly visible, similar to the small emulsion droplets that occurred in the phase behaviour tests (Figure 5.31). This shows a perfect example of related behaviour of different mixing conditions (turbulent mixing and laminar flow conditions).

The following figures show the phase behaviour at reservoir temperature conditions. The phase behaviour experiments SW, DW, SW200, SW1000, SW3000 and DW3000 which had reached

equilibrium after 72 hours at ambient temperature did not visibly change after being placed in the oven which confirms that they reached an equilibrium state as expected (Figure 5.33).

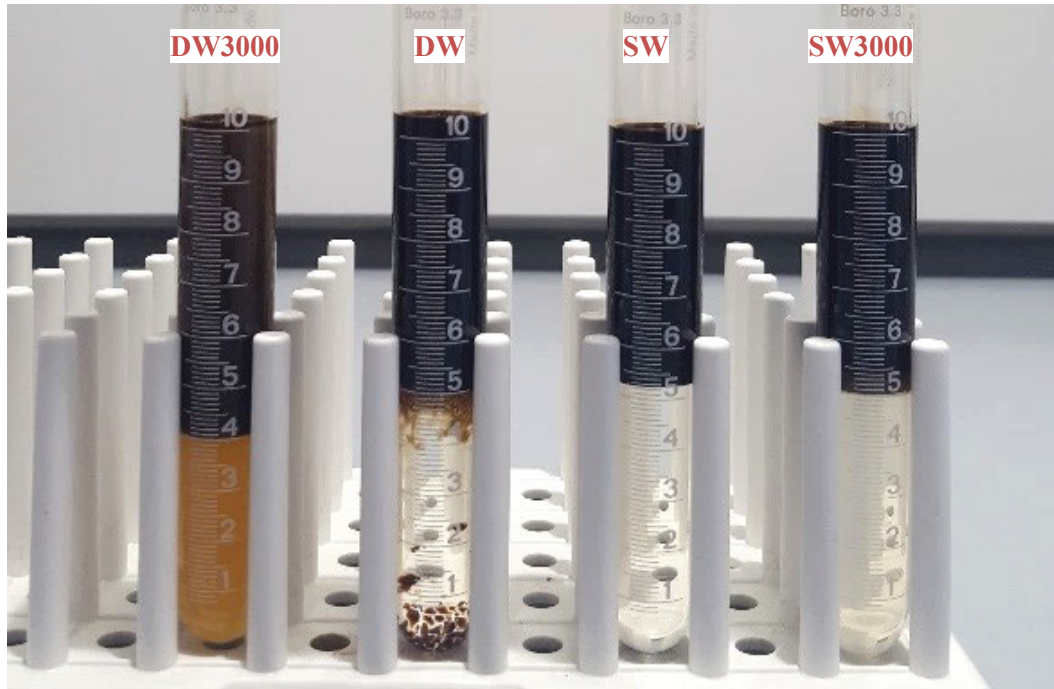


Figure 5.33 - Phase behaviour tests at reservoir temperature.

The oil swelling phase of SW3000 reduced a little in volume compared to ambient temperature conditions (Figure 5.29). The other displayed tests did not visible change, therefore the assumption that they have reached equilibrium is valid.

Figure 5.35 compares SW and SW3000 which reached equilibrium at ambient temperature with SW(60) and SW3000(60) which reached equilibrium in the oven after all of them were in the oven at 60°C for at least 72 hours.

The SW with oil looked the same whether it reached equilibrium at ambient temperature or in the oven while SW3000(60) showed a different colour in the water phase which suggests there additionally was O/W emulsion. Figure 5.35 further shows the microemulsion phase that formed around the 5ml mark with SW3000 and SW3000(60) in the oven. The emulsion of SW3000 was already visible at ambient conditions, although its colour slightly changed to a lighter tone as the total oil swelling amount reduced with temperature.

The phase behaviour test of DW3000(60) had more oil swelling and O/W than SW3000(60) as could be seen from the oleic phase volume and the darker shade of the water phase. DW3000 and DW3000(60) looked very much alike although DW3000 seemed to have a lighter coloured emulsion on top (6ml to 10ml mark).

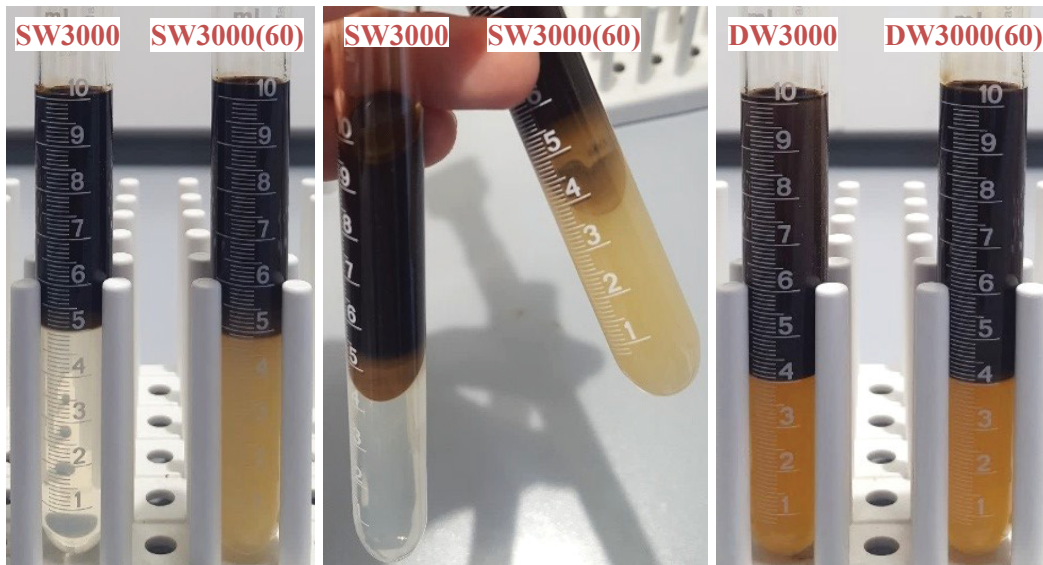


Figure 5.35 – Phase behaviour comparison of ambient and reservoir temperature equilibrium of 3000ppm.

Note that SW and 3000ppm formed a microemulsion between the aqueous and oleic phase and the main difference is that at 60°C there exists O/W while the water phase remained clear at ambient conditions. There was no visible difference between the behavior tests with DW.

During Exp. 10 (SW followed by SW3000 at 60°C) there was W/O and O/W emulsion formation visible, however, the grains were rather oil wet and if small emulsion bubbles formed they mostly snapped off the grain surface and moved into the oil or water emulsion phase.

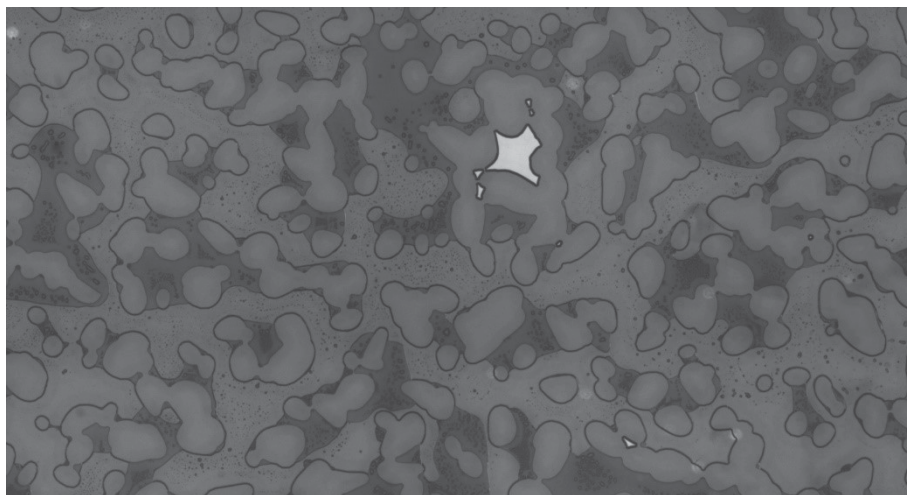


Figure 5.34 - Emulsion formation during Exp. 10 at 60°C.

There are emulsion bubbles visible in both, oil (dark grey) and water (light grey) phase.

In Exp. 11 (SW followed by DW3000 at 60°C) O/W, as well as W/O emulsion was detected and emulsion bubbles would get stuck to grain surfaces or at the front of the water front and either react further and dissolve into the water phase or become immobile.

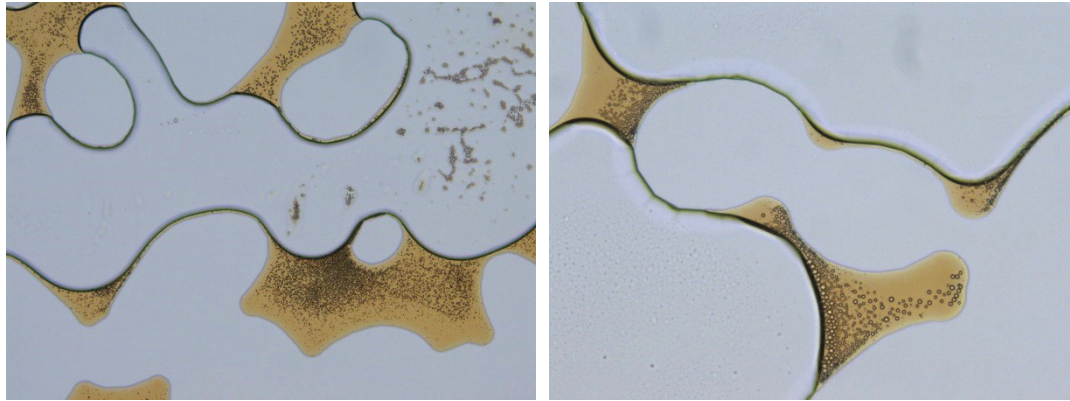


Figure 5.36 - Emulsion formation during Exp. 11 at 60°C.

In the left picture (magnification 10x) can be seen that both, O/W and W/O emulsions exist in the pore space. The right picture (magnification 20x) shows how emulsion bubbles accumulated on grain surfaces and the displacing fluid front.

Figure 5.37 compares SW5000(60) and SW12000(60) that reached equilibrium at reservoir conditions to each other and with SW5000 and SW12000.

The biggest oil swelling and W/O emulsion of all occurred in SW5000(60) (Figure 5.37).

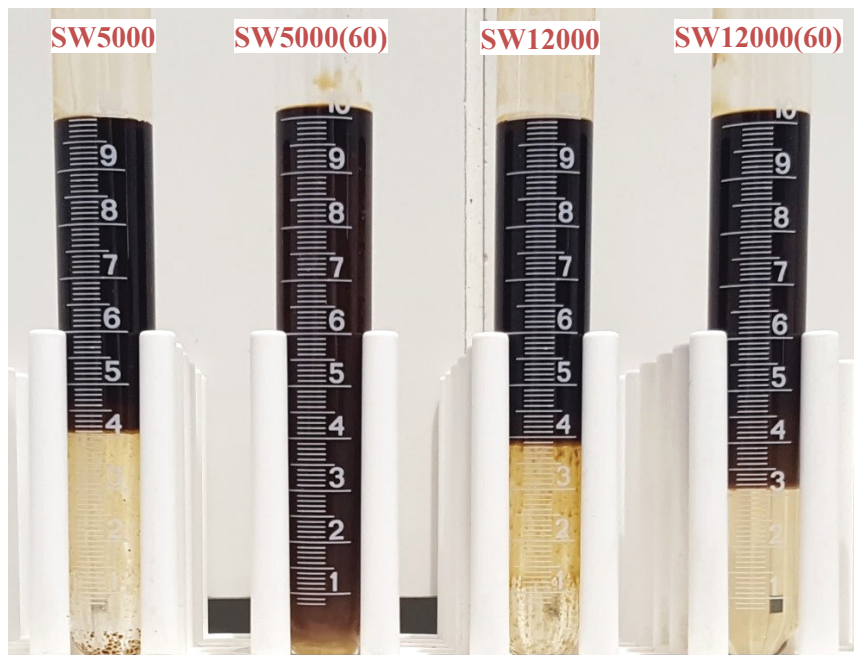


Figure 5.37 – Phase Behaviour comparison of ambient and reservoir temperature conditions for 5000ppm and 12000ppm.

Note that emulsion bubbles were sticking to the glass in the two tests at ambient temperature. These tests might not have reached equilibrium yet (after 72 hours) since these bubbles completely dissolved into the aqueous phase after they were heated (Figure 5.38).

SW12000(60) formed a larger oleic phase and W/O emulsion compared to its related test SW12000 which reached equilibrium at ambient temperature conditions. SW12000(60°C)



Figure 5.38 – Phase behaviour comparison at reservoir temperature conditions for 3000ppm to 12000ppm.

Note that the phase behavior tests which reached equilibrium at ambient temperature conditions (SW3000, SW5000 and SW12000) showed a trend of increasing oil swelling with increasing salinity and this trend was not represented by their corresponding tests at reservoir temperature. Different shades of brown in the oleic phase can be seen in the bottom pictures. A dark brown shade which looked like the pure crude oil was visible on top in the test tubes, in the middle an emulsion phase (light brown colour) of W/O and at the transition to the aqueous phase were small amounts of microemulsion visible by eye.

furthermore showed a relatively clear water phase and a quite stable emulsion phase in the middle (from 3ml to 4ml marker).

SW5000 and SW12000 had 72 hours in total to reach equilibrium at ambient conditions before they were placed in the oven with all other experiments. Both changed after only 48 hours in

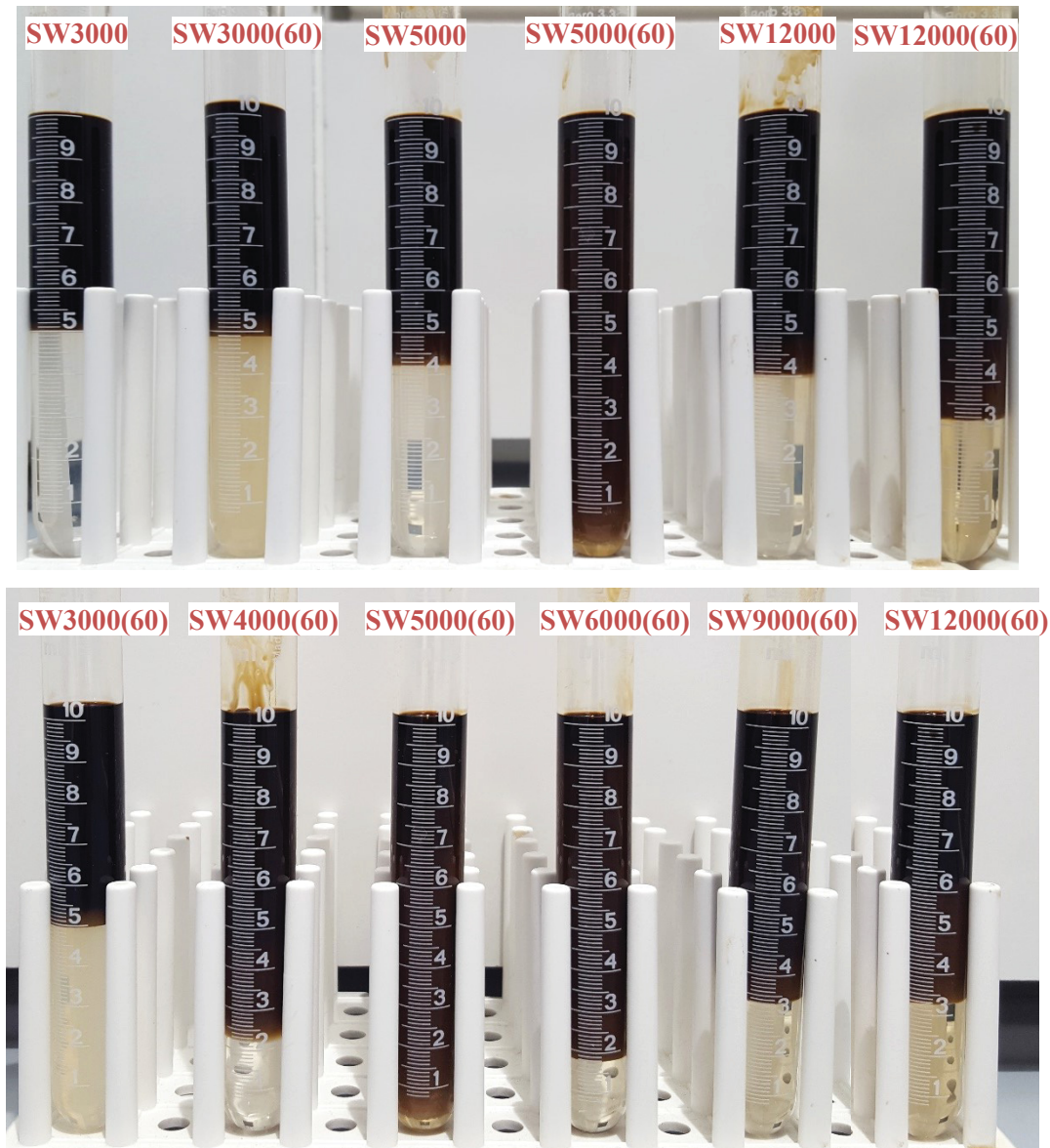


Figure 5.39 – Phase behaviour at reservoir temperature conditions with alkali concentrations from 3000ppm to 12000ppm (left to right).

Note that in the phase behavior tests which reached their equilibrium at reservoir temperature (bottom picture) oil swelling increased with increasing salinity up to a maximum at 5000ppm and then decreased with increasing salinity up to 12000ppm. Microemulsion (ME) phases between the oleic and aqueous phase were visible in all shown phase behavior tests by eye. The ME phase in SW4000(60) was particularly interesting as it showed a viscous fingering pattern into the above oleic emulsion phase which was visible by eye.

the oven as shown in Figure 5.38. They formed a clearer water phase after they were put in the oven at reservoir temperature (compared to Figure 5.37) and a microemulsion phase between oil and water.

At reservoir temperature conditions there could finally be found an optimum around 5000ppm in SW while at ambient temperature conditions a trend of minor oil swelling with higher concentration was observed. SW4000, SW6000 and SW9000 were only 48 hours in the oven up to this point, but it could already be seen that 4000 and 6000ppm looked quite similar and from 9000ppm to 12000ppm there were no visible changes.

Table 5.2 – Overview phase behaviour emulsion formation

Name	Emulsion at 23°C	Emulsion at 60°C	Name	Emulsion at 60°C
DW3000	O/W, W/O	O/W, W/O	DW3000(60)	O/W and W/O
SW3000	W/O	ME, O/W, W/O	SW3000(60)	ME, O/W, W/O
-			SW4000(60)	ME, W/O
SW5000	W/O	ME, W/O	SW5000(60)	ME, W/O
-			SW6000(60)	ME, W/O
-			SW9000(60)	ME, O/W, W/O
SW12000	W/O	ME, W/O	SW12000(60)	ME, O/W, W/O

5.5 Interfacial Tension

The interfacial tension was measured according to (Arnold, 2018) at 3000RPM and 20°C. The value for oil in DW was reviewed from (Arnold, 2018) as well as the value for DW with 3000ppm alkali concentration.

Table 5.3 - IFT at 20°C

Water	Alkaline concentration (Na ₂ CO ₃) [ppm]	IFT [mN/m]
DW	0	11-12
SW	0	0.4-0.5
SW	3000	0.35-0.4
DW	3000	0.12

The IFT in alkaline solution was in both cases (SW and DW respectively) smaller. The IFT of SW and SW3000 was not significantly different which correlates with the results of the flooding experiments where there was no additional recovery achieved in this combination (Exp. 4).

(Arnold, 2018) reported having trouble measuring oil in distilled water and considered the resulting values as unreliable. The measurements in DW and DW3000 were aimed to be re-measured but due to repeatedly instable droplet shapes this could not be achieved in a reliable way. Single oil droplets would stick together and would not allow realistic measurements (Figure 5.40).

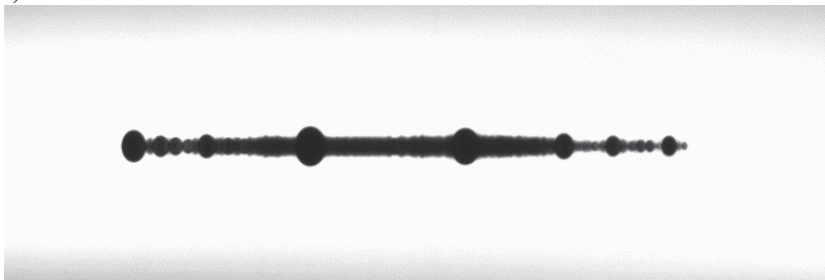


Figure 5.40 -- Spinning Drop DW3000

The measurements in SW3000 and SW worked both well on full droplets at 3000RPM.

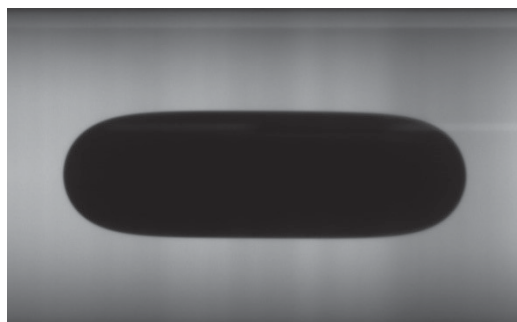


Figure 5.41 - Spinning Drop SW

SW in the work of (Arnold, 2018) had a different composition with more TDS. Figure 5.30 below shows a single IFT measurement of a full drop in SW3000. The single measurement value therefore was 0.375mN/m (top image in Figure 5.42).

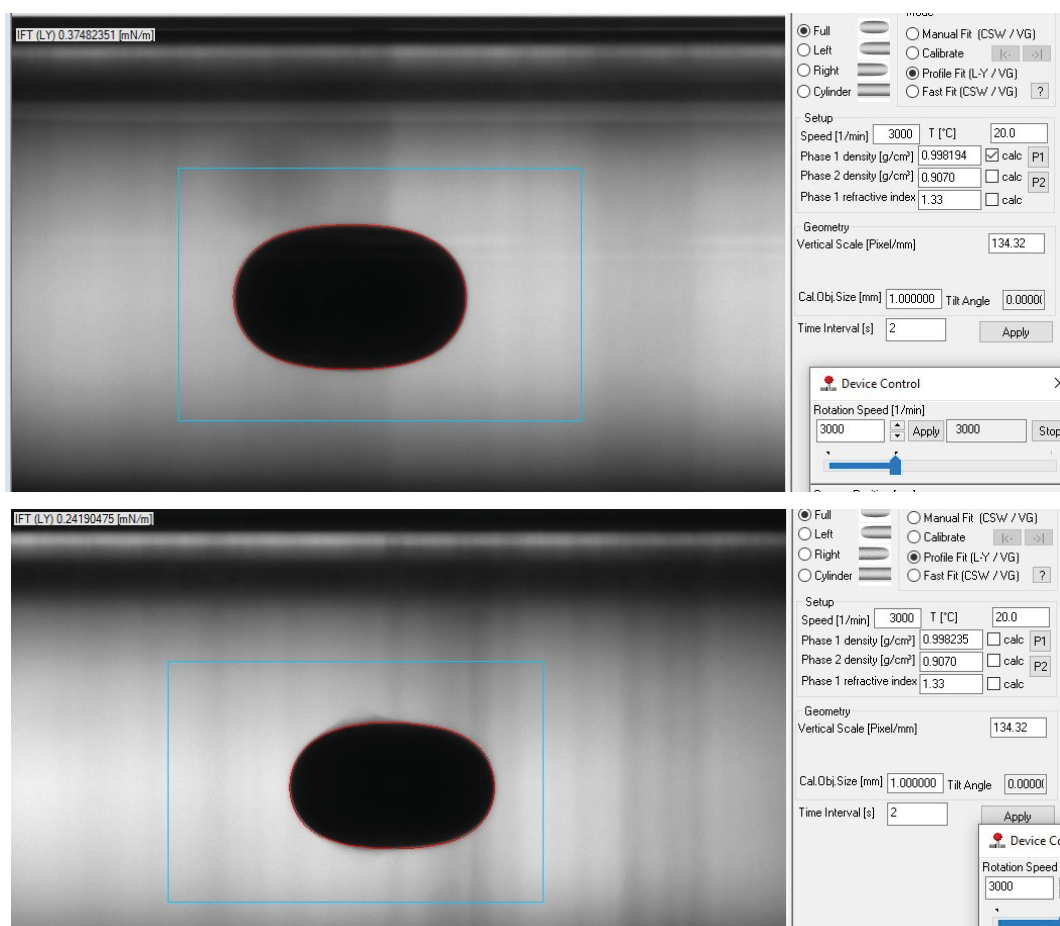


Figure 5.42 – Single IFT measurements of SW3000, top: 2 phase system, bottom: 3 phase system

This measurement was left running for several hours and later, on a different drop but at the same speed, there was a microemulsion detected (bottom image in Figure 5.42). This emulsion formation lead to an instable three phase system which resulted in a lower single measurement value of 0.24mN/m (Figure 5.42) and could not be further interpreted by conventional methods.

This result supports the statement that a microemulsion formation leads to an IFT reduction.

The complete time-dependent measurement can be found in Figure 5.43.

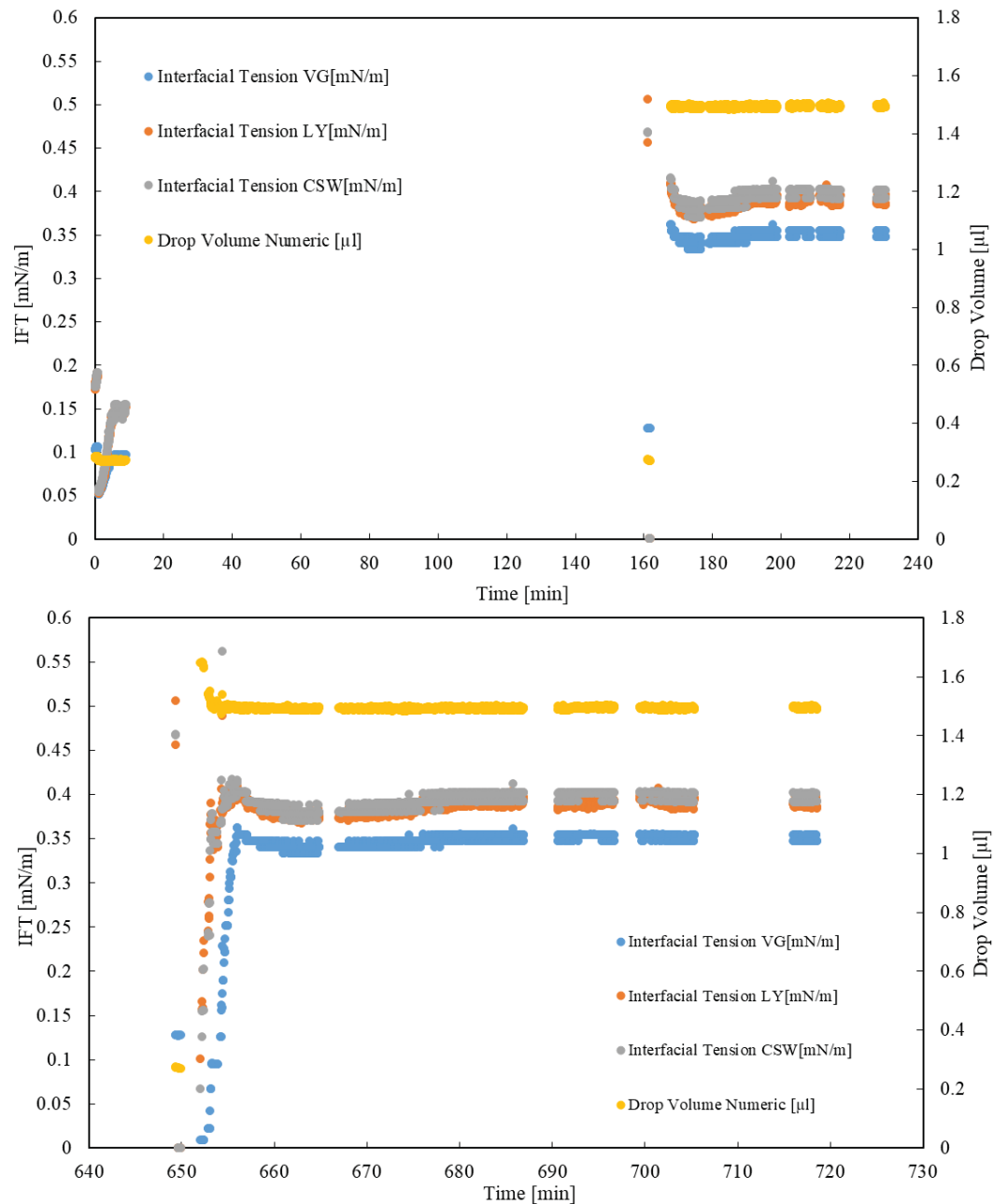


Figure 5.43 - IFT measurement SW3000 at 20°C

The IFT measurements for the alkaline concentrations of 200ppm and 1000ppm of SW were not considered since the phase behavior as well as the recovery in microfluidics did not show significant difference to the SW itself.

(Arnold, 2018) additionally measured IFT data dependent on temperature as shown in Figure 5.44. There was a temperature dependence visible for oil in synthetic water with 3000ppm

alkali. This could be expected to happen for the SW of this thesis in a similar way. The reservoir temperature of 60°C could not be measured with the currently available spinning drop setup.

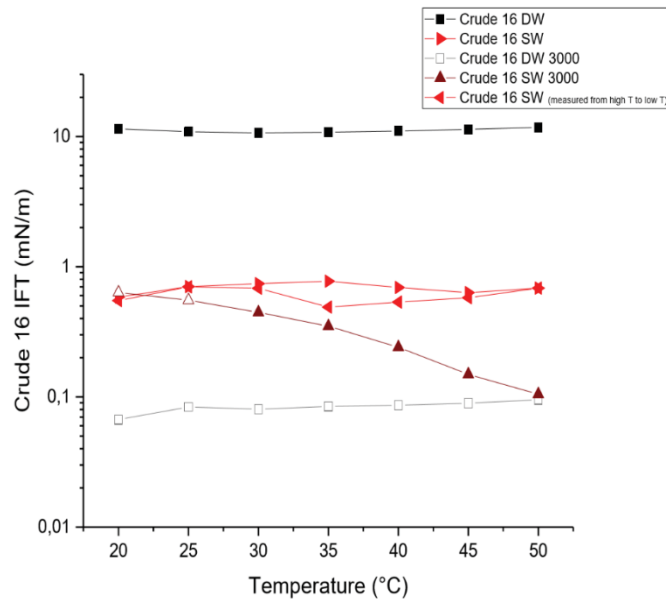


Figure 5.44 – Crude oil IFT Temperature dependence (Arnold, 2018)

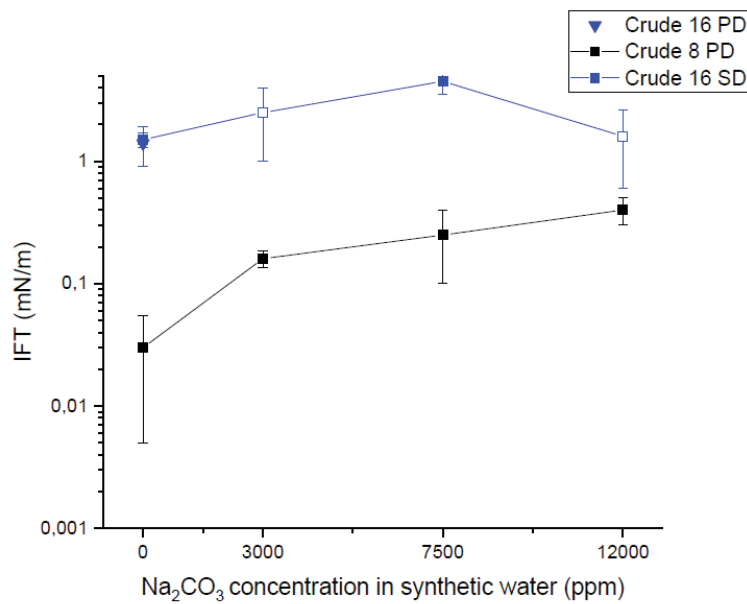


Figure 5.45 - IFT vs. Concentration in SW of (Arnold, 2018)

IFT measurements for 5000ppm and 12000ppm would be expected to show a similar behaviour compared to the work of (Arnold, 2018) in Figure 5.45. Since the SW used in this thesis contains less TDS than the synthetic water from (Arnold, 2018), the IFT would be expected to be lower than his result.

Chapter 6

Conclusion

6.1 Summary

In the frame of this thesis, displacement efficiency of oil by various alkaline solutions was studied by combining dynamic microfluidic experiments with observations on phase behavior tests. Experiments were carried out at ambient and reservoir temperature conditions of 60°C.

Generally, the results from all experiments were insightful and showed good repeatability. The temperature setup for microfluidic experiments was a good first approach. The target temperature of 60°C could be reached, if not completely equally distributed in the model which might have had an impact on the flooding pattern in the porous medium.

Regarding the water flooding experiments, the SW flooding experiments did produce a significantly higher amount of oil compared to the DW flooding.

There was no tertiary recovery achieved in alkaline flooding experiments with a concentration up to 3000ppm in SW. The combination of DW with alkaline salt (sodium carbonate) was the only experiment which caused a completely water-wet system during alkaline flooding by forming oil and emulsion droplets with low interfacial tension.

The highest ultimate recovery was achieved by the experiment with the highest concentration in this work (12000ppm in SW carried out at ambient temperature conditions) which was oil-wet in its final state after alkaline flooding.

The phase behavior experiments were in agreement with observations during dynamic flooding conditions in terms of emulsion formation. They provided a good overview of the present phases and how they might change under reservoir temperature conditions.

Microemulsion was only visibly generated in two dynamic alkaline flooding scenarios which both had DW3000 as alkaline flooding solution after DW (Exp. 5) and SW (Exp. 7) water flooding. All other dynamically created emulsions were O/W emulsions which finally lead to oil entrapment or W/O emulsions which were accumulating to grain surfaces or block the displacing fluid front. It must be kept in mind that these microfluidic experiments could only be evaluated in terms of fluid-fluid interactions since rock-fluid interactions, as they would appear in a real reservoir, were not considered.

The phase behavior study further showed that emulsion formation and swelling of the phases is dependent on salt and alkaline concentration as well as the temperature at which an equilibrium state is reached. An optimum state could be reached for SW around 5000ppm at reservoir temperature conditions resulting in maximum oil swelling. The according phase behavior experiments at ambient conditions showed no such optimum and their oleic phase volume increased with increasing alkali concentration.

The interfacial tension was reduced in the alkaline solutions compared to water, as expected. The difference in IFT reduction was much greater for DW and alkaline salt than SW and SW with alkaline salt which was also in agreement with the dynamic flooding experiments where the DW alkaline flooding experiment resulted in a completely water-wet system.

6.2 Future Work

The temperature setup for microfluidics could benefit from a higher quality solution, e.g. a fixed source of heat and simultaneous measurement of heat distribution.

The cleaning procedure of the micromodel, as well as first preparation of a new model, should be further improved to ensure equal conditions for each new experiment.

The micromodel itself could be improved by having separate inlets for oil saturation and for flooding experiments to ensure that oil in the tubes, valves or channels in front of the model inlet is not bypassed and flushed through the model at a later stage of flooding experiments.

For the oil used in this work, further IFT measurements and microfluidic experiments at reservoir temperature at concentrations above 3000ppm would be interesting since phase behaviour tests at reservoir temperature looked different from ambient temperature conditions.

Further studying microemulsion formation in general and its impact on oil production and performing alkaline-polymer flooding in microfluidics to study the effect on capillary and viscous forces.

Chapter 7

References

- Armstrong, R. T. et al., 2014. Critical capillary number: Desaturation studied with fast X-ray computed microtomography. *Geophysical Research Letters*, Band 41, pp. 55-60.
- Armstrong, R. T. et al., 2018. Porous Media Characterization Using Minkowski Functionals: Theories, Applications and Future Directions. *Transport in Porous Media*, pp. 1-31.
- Arnold, P., 2018. *Experimental investigation of interfacial tension for alkaline flooding*, s.l.: Montanuniversität Leoben.
- Borji, M., 2017. *Alkali-based Displacement Processes in Microfluidic Experiments: Application to the Matzen Oil Field*, s.l.: Montanuniversität Leoben.
- Clauset, A., Shalizi, C. R. & Newman, M. E. J., 2009. Power-Law Distributions in Empirical Data. *Society for Industrial and Applied Mathematics*, Band 51, pp. 661-703.
- Dullien, F. A. L., 1979. *Porous Media Fluid Transport and Pore Structure*. 1st Hrsg. s.l.: Academic Press.
- Gong, H. et al., 2016. Effect of wettability alteration on enhanced heavy oil recovery by alkaline flooding. *Colloids and Surfaces A: Physicochemical and Engineering Aspects*, Issue 448, pp. 28-35.
- International Energy Agency, 2018. *Energy Outlook 2018*, s.l.: s.n.
- Kharrat, A., 2018. *Alkali-based Displacement Processes in Microfluidic Experiments: Advanced Statistical Analyses*, s.l.: Montanuniversität Leoben.
- Lake, L. W., 2014. *Fundamentals of Enhanced Oil Recovery*. 2nd Hrsg. Richardson Texas: Society of Petroleum Engineers.

Li, M., Lin, M., Wu, Z. & Christy, A. A., 2005. The influence of NaOH on the stability of paraffinic crude oil emulsion. *Fuel*, 84(2-3), pp. 183-187.

Micronit, 2019. *Micronit microfluidics*. [Online] Available at: <https://store.micronit.com/microfluidic-chips/enhanced-oil-recovery-chips/3-pack-eor-chips-physical-rock-network-446> and <https://store.micronit.com/fluidic-connect-4515-chipholder>

[Accessed 21 January 2019].

Ott, H. et al., 2019. *Screening of EOR Potential on the Pore Scale - Application of Microfluidics to Alkaline Flooding*, Symposium of the Society of Core Analysts: held in Pau, France, August 2019, conference paper.

Sheng, J. J., 2011. *Modern Chemical Enhanced Oil Recovery: Theory and Practice*. 1st Hrsg. s.l.:Gulf Professional Publishing.

Sheng, J. J., 2014. A comprehensive review of alkaline-surfactant-polymer (ASP) flooding. *Asia-Pac. J. Chem. Eng.*, Band 9, pp. 471-489.

List of Figures

Figure 2.1 - Schematic Capillary Desaturation Curve (CDC) (Lake, 2014).....	15
Figure 2.2 - Ternary diagram for Winsor types II and III.	17
Figure 3.1 - Left: Physical Rock Model Right: Chip holder (Micronit, 2019)	19
Figure 3.2 - Schematic Experimental Setup.....	20
Figure 4.1 – Oil Saturated Micromodel	25
Figure 4.2 – Colour picture of fluorescent light modus during a waterflooding experiment ..	27
Figure 4.3 – Binarized outcrop of the oil saturated micromodel.	28
Figure 4.4 – Cluster Volume and Lorenz Analysis.....	29
Figure 4.5 – Example “Cluster Analysis” plot (top) and example Lorenz Plot (bottom).	30
Figure 4.6 – Sub volumes of the micromodel at different stages of flooding experiments.	32
Figure 4.7 - Binarized images of Figure 4.6	32
Figure 5.1 - Time dependent RF of water flooding scenarios.....	36
Figure 5.2 – Water flooding displacement patterns with a time interval of 20min.....	37
Figure 5.3 - SW anomalous displacement pattern in Exp. 6.	38
Figure 5.4 – Final states after water flooding with SW: a) Exp. 3, b) Exp. 7, c) Exp. 2, d) Exp. 4	39
Figure 5.5 – SW flooding of Exp. 2, 3, 4 and 7 a) Lorenz Plot and b) Cluster Analysis.....	39
Figure 5.6 – a) Exp. 7 after SW, b) Exp. 5 after DW, c) Lorenz Plot, d) Cluster Analysis	40
Figure 5.7 - left: Exp. 12 after SW flooding, right: Exp. 13 after SW flooding	40
Figure 5.8 – Exp. 12 and 13 SW: a) Lorenz plot and b) Cluster Analysis.....	41
Figure 5.9 - SW flood Exp. 7 and Exp. 13 Cluster Analysis	41
Figure 5.10 - Lorenz Plot of Water flooding	42
Figure 5.11 – Ultimate Recovery vs. PV injected and total ionic strength (TIS)	43
Figure 5.12 - Alkalinity effect on tertiary recovery.	44
Figure 5.13 – Top: Concentration effect on tertiary recovery (circle markers) and normalized Euler characteristic (triangular markers).....	45
Figure 5.14 - Exp. 13 a) after water flooding, b) after alkaline flooding.....	46
Figure 5.15 – Exp. 13 a) Lorenz Plot, b) Cluster Analysis	47
Figure 5.16 - Exp. 5 a) after DW flooding, b) after DW and DW3000 flooding.....	48
Figure 5.17 - Exp. 5: a) Lorenz Plot, b) Cluster Analysis compared to Exp. 13	49
Figure 5.18 - Exp. 12: a) after water, b) after alkaline flooding	50
Figure 5.19 – a) Lorenz Plot Exp. 12, b) Cluster Analysis Exp. 12 and Exp. 13.....	51
Figure 5.20 – Exp 7: a) Water Break Through (WBT) b) after SW c) after SW and DW3000	52
Figure 5.21 – Exp. 7: a) Lorenz plot, b) Cluster Analysis compared to Exp. 5	53
Figure 5.22 - Exp. 6: a) after SW, b) after SW3000, c) Lorenz plot, d) Cluster Analysis	54
Figure 5.23 - Exp. 2: a) after SW, b) after SW200, Exp. 3: c) after SW, d) after SW1000, Exp. 4: e) after SW, f) after SW3000	55
Figure 5.24 - Lorenz Plot and Cluster Analysis.....	56
Figure 5.25 - Cluster Analysis: alkaline flooding comparison after SW flooding.....	57
Figure 5.26 - Exp. 10 at 60°C: a) after SW, b) after SW3000, Exp. 11 at 60°C: c) after SW, d) after DW3000	57
Figure 5.27 - Exp. 11 water flooding at reservoir temperature conditions	58
Figure 5.28 - Lorenz Plot and Cluster Analysis Exp. 10: a) & b), Exp. 11: c) & d).....	59
Figure 5.29 - PB at ambient temperature (0ppm to 3000ppm)	60
Figure 5.30 - Emulsion formation during Exp. 5 (top) and during Exp. 7 (bottom).....	61
Figure 5.31 – PB at ambient temperature (3000ppm to 12000ppm).....	62
Figure 5.32 - Emulsion formation (Magnification 10x and 20x): a) & b) Exp. 12, c) & d) Exp. 13	63
Figure 5.33 - Phase behaviour tests at reservoir temperature.	64

Figure 5.34 – Phase behaviour comparison of ambient and reservoir temperature equilibrium of 3000ppm.	65
Figure 5.35 - Emulsion formation during Exp. 10 at 60°C.....	65
Figure 5.36 - Emulsion formation during Exp. 11 at 60°C.....	66
Figure 5.37 – Phase Behaviour comparison of ambient and reservoir temperature conditions for 5000ppm and 12000ppm.....	66
Figure 5.38 – Phase behaviour comparison at reservoir temperature conditions for 3000ppm to 12000ppm.	67
Figure 5.39 – Phase behaviour at reservoir temperature conditions with alkali concentrations from 3000ppm to 12000ppm (left to right).....	68
Figure 5.40 -- Spinning Drop DW3000	70
Figure 5.41 - Spinning Drop SW	71
Figure 5.42 – Single IFT measurements of SW3000, top: 2 phase system, bottom: 3 phase system	71
Figure 5.43 - IFT measurement SW3000 at 20°C	72
Figure 5.44 – Crude oil IFT Temperature dependence (Arnold, 2018)	73
Figure 5.45 - IFT vs. Concentration in SW of (Arnold, 2018)	73

List of Tables

Table 3.1 - Physical Rock Network Specifications (Micronit, 2019).....	20
Table 4.1 - Oil properties	23
Table 4.2 – Synthetic Brine (SW) Composition	23
Table 4.3 - Prepared Injection Fluids.....	24
Table 4.4 - Overview Microfluidic Experiments	25
Table 4.5 - Overview Phase Behaviour Experiments	33
Table 4.6 - Spinning Drop Input Parameters	34
Table 5.1 – Results: Recovery Factor and normalized Euler number.....	35
Table 5.2 – Overview phase behaviour emulsion formation	69
Table 5.3 - IFT at 20°C	70